Original Article

Half-a-century (1971–2020) of glacier shrinkage and climatic variability in the Bhaga basin, western Himalaya

DAS Suresh[1] https://orcid.org/0000-0003-4148-8551; e-mail: suresh41_ssf@jnu.ac.in

SHARMA Milap Chand[1] https://orcid.org/0000-0003-4681-6745; e-mail: milap@jnu.ac.in

MURARI Madhav Krishna[2] https://orcid.org/0000-0001-5217-2275; e-mail: madhav.iuac@gmail.com

NÜSSER Marcus[3, 4*] https://orcid.org/0000-0002-8626-8336; ✉ e-mail: marcus.nuesser@uni-heidelberg.de

SCHMIDT Susanne[3] https://orcid.org/0000-0002-6200-4539; e-mail: s.schmidt@uni-heidelberg.de

*Corresponding author

1 Centre for the Study of Regional Development, Jawaharlal Nehru University, New Delhi 110067, India

2 National Geochronology Facility, Inter-University Accelerator Centre, New Delhi 110067, India

3 Department of Geography, South Asia Institute (SAI), Heidelberg University, Heidelberg 69115, Germany

4 Heidelberg Centre for the Environment (HCE), Heidelberg University, Heidelberg 69120, Germany

Abstract: Glacier shrinkage is a globally occurring phenomena. High-resolution change detection based on frequent mapping and monitoring of high-altitude glaciers is necessary to precisely evaluate future water availability and to understand glacier evolution under different climatic scenarios in the Hindukush-Karakoram-Himalayan (HKH) region. This also holds true for the Bhaga basin of the western Himalaya. This study investigates glacier and glacier lake changes in the Bhaga basin, over the last five decades based on satellite imagery including Corona KH4 (1971), Landsat 7 Enhanced Thematic Mapper Plus (ETM+; 2000), Linear Imaging Self-Scanning Sensor (LISS IV; 2013), and Sentinel 2 (2020). Regional temperature and precipitation trends were evaluated from gridded climatic datasets (1900–2020). In the Bhaga basin 306 glaciers (>0.2 km²) were mapped with a total area of 360.3 ± 4.0 km², of which 55.7 ± 0.6 km² was covered with debris in 2013. The total glacier covered area decreased by ~8.2 ± 1.5 % (0.16 ± 0.03 % yr⁻¹) during the entire observation period 1971–2020, with noticeable heterogeneity between tributary watersheds. In the past two decades (2000–2020), the deglaciation rate has increased significantly (0.25 % yr⁻¹) compared to the previous decades (1971–2000; 0.12 % yr⁻¹). Glacier lake area increased by 0.6 ± 0.1 km² (0.012 km² yr⁻¹) between 1971 and 2020. The NCEP/NCAR climatic data reveals an increase of 0.63°C in temperature and a decrease of 6.39 mm in precipitation for the period 1948–2018. In comparison, APHRODITE data shows an increasing trend in temperature of 1.14°C between 1961 and 2015 and decreasing trend in precipitation of 31 mm between 1951 and 2007. Both NCEP/NCAR and APHRODITE data reveal significant temperature increase and precipitation decrease since the 1990s, which have probably augmented ice loss in the Bhaga basin during the early 21st century.

1 Introduction

Mountain glaciers are considered one of the best indicators of climate change. The Hindu Kush-Karakoram-Himalaya (HKH) has the largest ice mass outside the polar regions, replenishing the major river systems of South and Southeast Asia (Immerzeel et al. 2010; Bolch et al. 2012; Armstrong et al. 2019). Therefore, Himalayan glacier changes are of great concern and have been the subject of debates over the last few decades (Nüsser and Baghel 2014; Bolch et al. 2019). Like in other regions of the world, Himalayan glaciers have been in a general state of recession since the Little Ice Age (Mayewski and Jeschke 1979; Chand et al. 2017; Rowan 2017; Hock et al. 2019), except for an emerging indication of stability or mass gain in the Karakoram region (Hewitt 2005, 2011; Kääb et al. 2015; Farinotti et al. 2020) and in the Astore basin of the northwestern Himalaya (Muhammad et al. 2019). Glaciers in the central Himalaya from Uttarakhand to Bhutan are receding at different rates than in the western Himalaya (Table 1). Climatic differences between monsoonal- and westerly-dominated Himalayan regions as well as cold–arid regions control glacier loss at the regional scale (Hewitt 2005, 2011; Immerzeel et al. 2010; Schmidt and Nüsser 2017). Studies have reported that heterogeneous glacier shrinkage across the Himalayan region is mainly controlled by the interplay between local topographical settings and increasing temperatures (Immerzeel et al. 2010; Salerno et al. 2017). Several topographical (slope, elevation, aspect) and morphological (debris cover, glacier lakes) factors control glacier loss at the local scale (Brun et al. 2019; Scherler et al. 2011a, b; Salerno et al. 2017). The present study investigates glacier changes in the entire Bhaga basin, one of the largest tributaries of Chandra River in the western Himalaya. This study area contains more than 300 glaciers, located in different elevations and orientations, which debris coverage vary between 0% and 50% of the total glacierized area. Thus, it provides an opportunity to examine the role of surface morphology on glacier changes in a transitional climatic zone.

Until now, only few studies have been published on glacier surface area changes in the entire Bhaga basin based on remote sensing approaches (Birajdar et al. 2014; Das and Sharma 2019; Kaushik et al. 2020)

and no study addresses such changes together with associated variables such as debris cover, topography, and changes of precipitation and temperature. Kulkarni et al. (2007, 2011) used the Survey of India (SoI) topographical maps and Kaushik et al. (2020) used Landsat Multispectral Scanner System (MSS; 1979) imagery with low spatial resolution and Sentinel 2 (2017) images to investigate changes of 48 glaciers (Table 1). However, on the coarser-resolution satellite datasets (e.g., Landsat MSS), the identification of debris-covered glacier tongues is difficult. The declassified panchromatic, high spatial resolution imagery of Corona and Hexagon acquired in the 1960s and 1970s provide an outstanding possibility to extract former glacier outlines and to compare them with contemporary glacier outlines derived from satellite imagery (Bhambri et al. 2011; Schmidt and Nüsser 2012; Chand and Sharma 2015; Schmidt and Nüsser 2017; Das and Sharma 2019; Nüsser and Schmidt 2021). Das & Sharma (2019) investigated glacier surface area changes in the Jankar Chhu watershed (JCW), a tributary of Bhaga basin, based on Corona (1971) and Sentinel 2 (2016) images.

This study aims to achieve the following objectives: (i) to generate a field survey supported glacier inventory for the entire Bhaga basin using high-resolution (5 m) images from Linear Imaging Self-Scanning Sensor (LISS) IV (2013); (ii) to assess multitemporal glacier changes based on remote sensing datasets for the period 1971–2020; (iii) to evaluate climatic trends during the last century (1900–2020), and (iv) to assess the potential role of topographic and climatic variables on heterogeneous ice loss.

2 Study Area

The Bhaga basin is located in the Western Himalaya and covers an area of about 1657 km^2 (Fig. 1a). Bhaga River forms a major northern tributary of the Chandra River and originates from Suraj Tal near Baralacha La and confluences with Chandra near Tandi Village (Fig. 1b). The two main tributaries Jankar Chhu and Milang join the main Bhaga River at Darcha (32.67° N, 77.19° E). The elevation of the Bhaga basin ranges from 2860 to 6430 m a.s.l.

Table 1 Assessment of glacier recessions in the Himalayas.

Regions/ Basins	Period	No./Area of glaciers investigated	Change (%)	Rate of change (% yr^{-1})	Dataset used	References
Trans Himalaya						
Kang Yatze Massif, Ladakh	1969–2010	82/181 km² in 2002	14.3	0.3	Corona, SPOT	Schmidt and Nüsser 2012
Ladakh range	1991–2014	864/402 km² in 2002	12.8	0.6	Corona, Landsat	Chudley et al. 2017
Zanskar basin	1962–2001	671/929 km² in 2001	9.0	0.2	SoI maps, LISS III	Kulkarni et al. 2011
Western Himalaya						
Ravi basin	1971–2013	285/164.5 km² in 2002	4.6	0.1	Corona, Landsat	Chand and Sharma 2015
Saraswati/ Alaknanda	1968–2006	83/311 km² in 2006	4.6	0.1	Corona, ASTER	Bhambri et al. 2011
Bhagirathi	1968–2006	20/274 km² in 2006	5.7	0.2		
Chenab basin	1962–2001	359/1110 km² in 2001	21.3	0.5	SoI maps, LISS III	Kulkarni et al. 2007
Parbati basin	1962–2001	88/379 km² in 2001	22.1	0.5		
Baspa basin	1962–2001	19/140 km² in 2001	19.4	0.5		
Goriganga basin	1962–2001	41/269 km² in 2001	19.2	0.5	SoI maps, LISS III	Kulkarni et al. 2011
Bhagirathi basin	1962–2001	212/1178 km² in 2001	14.0	0.3		
Chandra basin	1962–2001	116/554 km² in 2001	20.1	0.5		
Bhaga basin	1962–2001	111/254 km² in 2001	30.2	0.7		
Miyar basin	1962–2001	166/523 km² in 2001	8.0	0.2		
Bhut basin	1962–2001	189/420 km² in 2001	10.1	0.2		
Warwan basin	1962–2001	253/672 km² in 2001	21.0	0.5		
Chandrabhaga basin	1980–2010	15/368 km² in 2010	2.5	0.1	Landsat MSS, OLI	Pandey and Venkataraman 2013
Baspa basin	1976-2011	109/187 km² in 2011	18.1	0.4	Landsat MSS, OLI	Mir et al. 2017
Kashmir Himalaya	1980–2013	9/24 km² in 2013	17.9	0.5	Landsat	Murtaza and Romshoo 2017
Bhaga basin	1979-2017	45/231 km² in 2017	3.0	0.1	Landsat MSS, OLI	Kaushik et al. 2020
Miyar basin	1989–2014	29/ 218 km² in 2014	9.0	0.4	Landsat MSS, OLI	Patel et al. 2018
Jankar Chhu	1971-2016	127/181 km² in 2016	7.5	0.2	Corona, Landsat, Sentinel 2A	Das and Sharma 2019
Bhaga basin	1971–2020	306/360 km² in 2013	8.2	0.2	Corona, LISS IV, Landsat	Present Study
Central and Eastern Himalaya						
Kumbhu Himalaya	1962–2005	3/87 km² in 2005	5.2	0.1	Corona, ASTER, Landsat	Bolch et al. 2008
Kanchenjunga–Sikkim area	1962–2000	487/1463 km² in 2002	19.0	0.5	Corona, Landsat	Racoviteanu et al. 2015
Sikkim Himalaya	1989/90–2010	39/333 km² in 1989	3.3	0.2	Landsat, LISS III	Basnett et al. 2013
Bhutan Himalaya	1980–2010	885/642 km² in 2010	23.3	0.8	Landsat ETM+	Bajracharya et al. 2014

Notes: SoI- Survey of India topographic maps; MSS- Multispectral Scanner; ETM+ - Enhanced Thematic Mapper; OLI – Operational Land Imager; LISS - Linear Imaging Self-Scanning Sensor; ASTER - Advanced Spaceborne Thermal Emission and Reflection Radiometer; SPOT - *Satellite* Pour l'Observation de la Terre.

For a detailed analysis of glacier change patterns, the entire Bhaga basin was divided into four watersheds (Fig. 1b): Bhaga lower watershed (BLW), Jankar Chhu watershed (JCW), Bhaga upper watershed (BUW), and Milang Valley (MV). The JCW forms the largest (690 km²) and MV the smallest (292 km²) of these four watersheds.

Located in the rain shadow of the monsoon-dominated Pir-Panjal range to the south and the westerly-dominated Trans-Himalaya to the north, the Bhaga basin is characterized by a strong N-S precipitation gradient. Seasonal distribution of precipitation is influenced by two major circulation systems: (1) mid-latitude Westerlies in the winter months and (2) South Asian Monsoon in the summer months. All months are characterized by humid conditions, with two peaks of precipitation (> 80 mm) in March and July (Fig. 1c, d) and a minimum in

November (< 15 mm). More than 80% of precipitation occurs as snowfall (Das and Sharma 2019; Das et al. 2022). Average monthly summer (July-August) temperatures range from 4°C to 10°C, while average
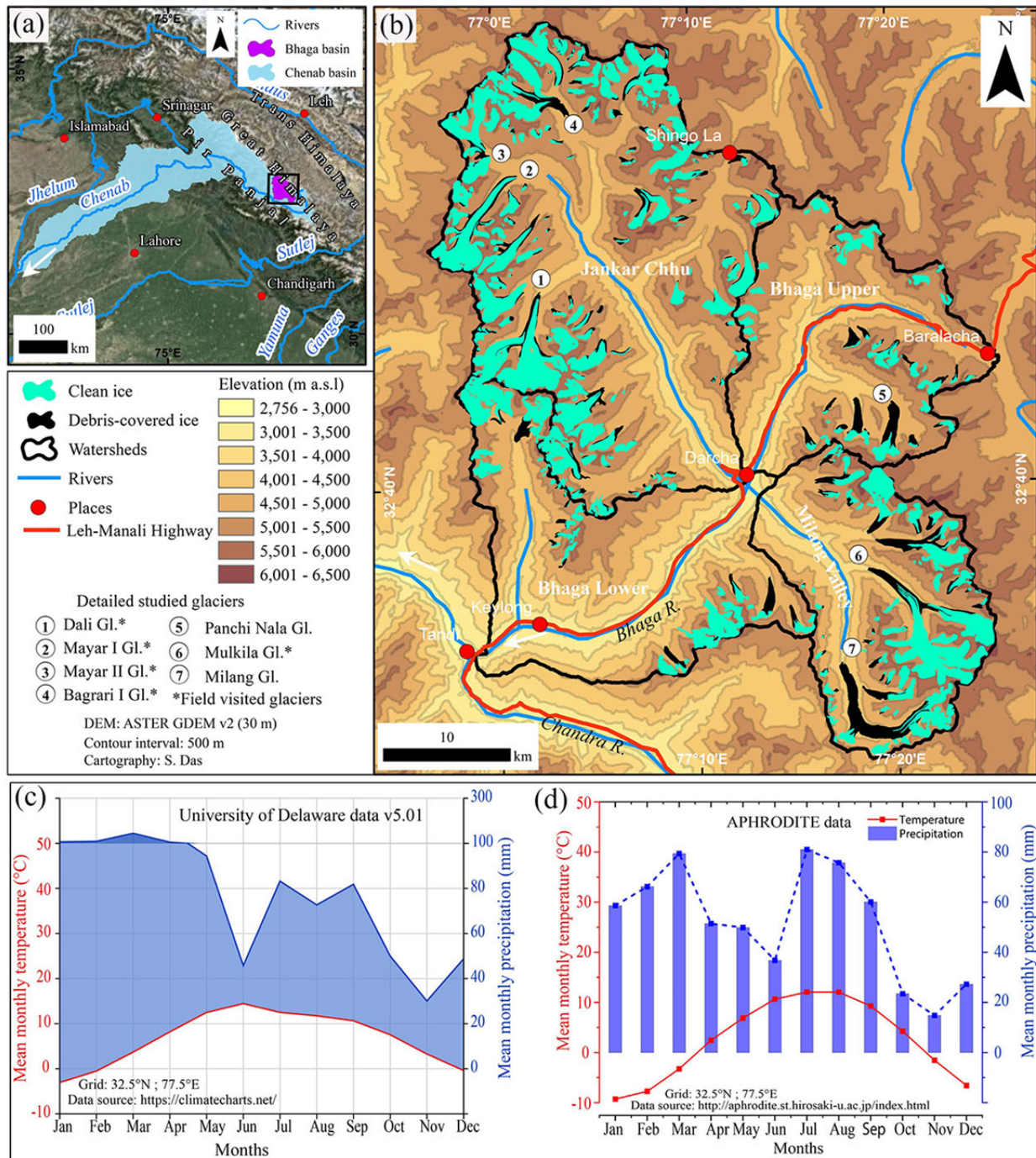
Fig. 1 (a) Location of the study area in the upper Chenab basin in the Western Himalaya. (b) Glacier coverage in the Bhaga basin based on LISS IV (23 Oct 2013) images. The entire Bhaga basin is categorized into four watersheds (i.e., Bhaga lower, Jankar Chhu, Bhaga upper, and Milang valley) for detailed analysis. Elevation of the region is shown in background based on the ASTER GDEM v2 (30 m). Elevation is categorized into 500 m altitude bands. The elevation of the Bhaga basin ranges from 2860 to 6430 m a.s.l. (c) Walter-Lieth climatic diagram of the Bhaga basin (grid: 32.5°N and 77.5° E) based on University of Delaware gridded dataset (https://climatecharts.net/). Light and dark blue shaded areas depict prevailing humid and per-humid conditions, respectively. (d) Mean monthly temperature (1961-2007) and precipitation (1951-2015) for the Bhaga basin derived from APHRODITE data. Two peaks in precipitation show the influence of mid-latitude westerlies in winter and south Asian monsoon in summer months.

winter temperatures (December-February) range from −2°C to −9°C (Fig. 1c, d).

3　Data and Methods

3.1 Field mapping

Multiple field observations and mapping campaigns were carried out for selected glaciers in the Bhaga basin between 2015–2020. Field visits were mostly carried out during the ablation seasons between August and October. Terminus characteristics (i.e., snout position at the center of the terminus, stagnant ice bodies, thickness of debris cover, ice temperature) were mapped using handheld GPS (Garmin etrex10; ±5 m horizontal accuracy; Fig. 2). Frontal characteristics of four glaciers (i.e., Dali, Mayar I and II, Bagrari) in the JCW were monitored during field visits (Appendixes 1-4). Furthermore, field photographs were taken to validate remote sensing datasets, especially for debris-cover mapping. Snow and glacier conditions (e.g., existing snowfields and avalanche cones) were recorded during field visits.

3.2 Image collections and rectifications

Five forward Corona strips were used to map the 1971 glacial extents (Table 2). All subsets were georeferenced and terrain corrected based on two operational approaches: (1) projective transformation was performed based on ground control points (GCPs) acquired from the base image (Sentinel 2A (2016), Level 1C) and Advanced Spaceborne Thermal Emission and Reflection Radiometer Global Digital

Elevation Model (ASTER) GDEM v2 in ERDAS Imagine 14; followed by (2) spline adjustment in ESRI ArcGIS 10.2 (Chand and Sharma 2015; Das and Sharma 2019) (Table 2). The Landsat ETM+ (2000) was pan-sharpened using the Brovey transformation image fusion techniques and co-registered to the Sentinel image based on a projective transformation. High-resolution LISS IV images from 2013 and Sentinel 2B images from 2020 were co-registered to the base image using the "Auto Sync workstation" available in ERDAS Imagine. The Sentinel 2B image from 2020 was used to map the latest glacier outlines. For glacier mapping, the shortwave infrared bands (band 11 and 12; 20 m spatial resolution) of Sentinel 2 were resized to 10 m (Das and Sharma 2019).

3.3 Glacier area and terminus change

3.3.1 Area mapping and inventory

The identification and mapping of glaciers from satellite images can be conducted using semi-automatic techniques (Paul et al. 2013) or through manual delineation (Bhambri et al. 2011; Schmidt and Nüsser 2012; Das and Sharma 2019). Band ratio techniques are a well-established method for clean ice mapping from satellite data (Paul et al. 2013; Racoviteanu et al. 2015), although debris-covered ice mapping using automatic methods is still problematic (Scherler et al. 2018; Herreid and Pellicciotti 2020). To establish the best approach, both semi-automatic and manual digitization were tested in the present study. The most commonly used band ratios from Landsat images are red/SWIR1 (Bolch et al. 2010) and NIR/SWIR1 for clean ice mapping (Paul et al. 2013; Appendix 5). The band ratio red/SWIR2 was

Table 2 Detail of the dataset used in this study.

| +Data Acq.	Sensor	Scene ID/ Path-Row	++Spatial resol. (m)	Bands	No of GCPS	RSME (pixel)	*Horiz. Accu. (m)
28.09.1971	Corona KH-4B	DS1115-2282DF058	1.83 in the center	Pan	40	0.3	5.2
	Corona KH-4B	DS1115-2282DF059			275	0.2	5.4
	Corona KH-4B	DS1115-2282DF060			320	0.2	6.2
	Corona KH-4B	DS1115-2282DF061			25	0.1	6.1
	Corona KH-4B	DS1115-2282DF062			20	0.1	7.2
15.10.2000	Landsat ETM+	LE71470372000289SGS00	15, 30	Pan, VIS+MIR	318	0.4	10.5
23.10.2013	LISS IV	094_047_143034711	5	VIS	264	0.3	1.8
	LISS IV	095_048_143034721			510	0.3	1.8
02.10.2016	Sentinel 2	L1C__20161002T104830_T43SFS	10, 20	VIS, SWIR		Base image	
28.08.2018	Sentinel 2	L1C_T43SFS_20180828T053642	10, 20	VIS, SWIR	526	0.3	< 1.0
11.10.2020	Sentinel 2	L1C_T43SFS_A027701_20201011T053056	10, 20	VIS, SWIR	320	0.3	< 1.0

Notes: +Date Acq.: Data acquisition; ++Spatial resol.: Spatial resolution; *Horz. Accu.: Horizontal Accuracy.
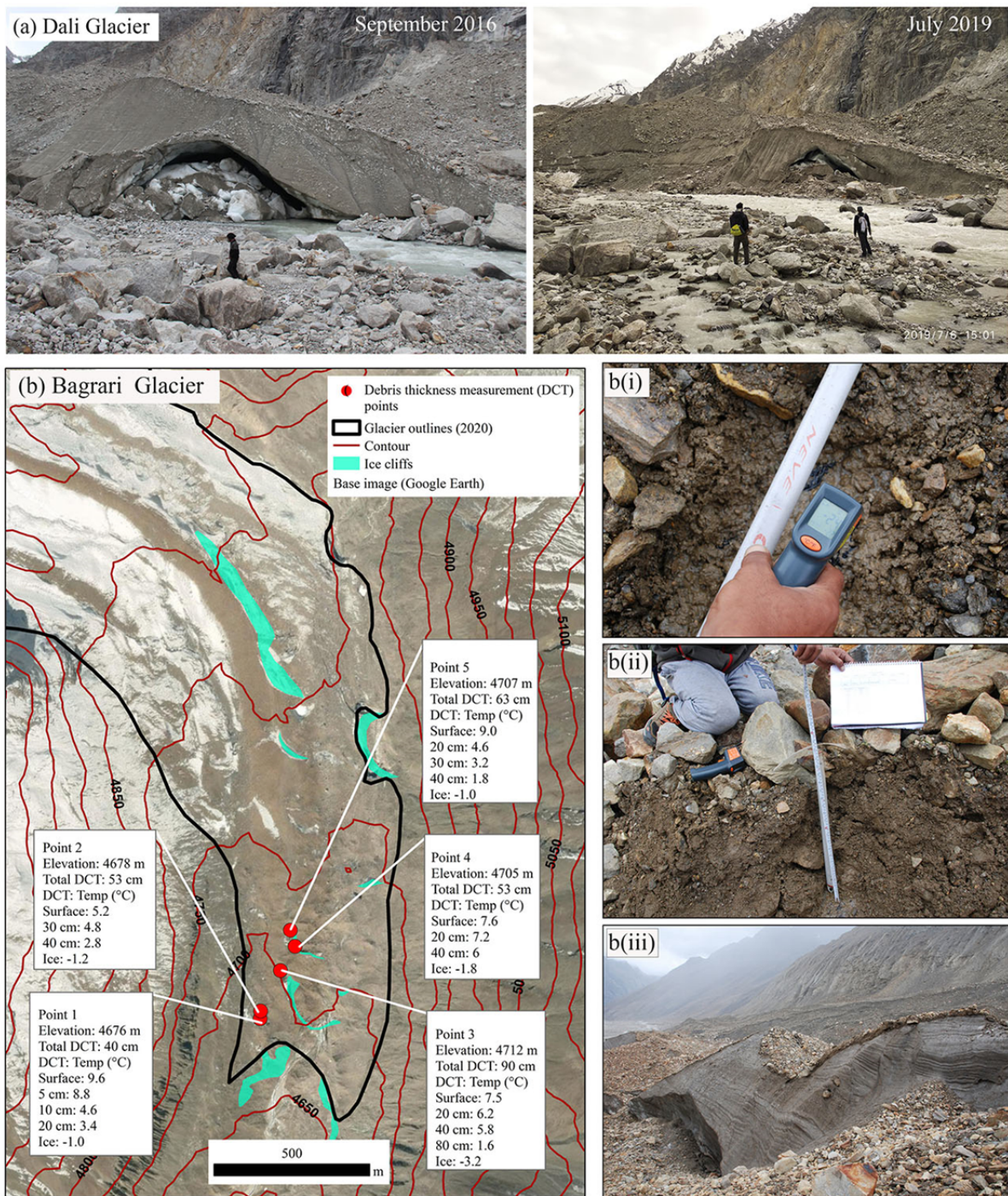
Fig. 2 (a) Repeated photographs of Dali glacier's snout in the Bhaga basin in 2016 and in 2019. (b) Characteristics of ablation zone of debris-covered Bagrari I Glacier in the JCW. Measurements of debris thickness and underlying ice temperature on Bagrari I glacier. Temperature was measured using a handheld IR thermometer (b(i)). Debris thickness was measured using a measuring tape (b(ii)). Enhanced melt in association with exposed ice cliffs produces supraglacial depression (b(iii)). For the location of glaciers in the Bhaga basin, see Fig. 1b.

tested with a threshold value of 2.2 for Sentinel 2 (Appendix 5) and red/SWIR1 with a threshold value of 2.1 for Landsat (Appendix 6) in order to map clean ice. Normalized difference snow index (NDSI = $B_{Green} - B_{SWIR}/B_{Green} + B_{SWIR}$) and normalized difference glacier index (NDGI = $B_{Green} - B_{Red}/B_{Green} + B_{Red}$) were
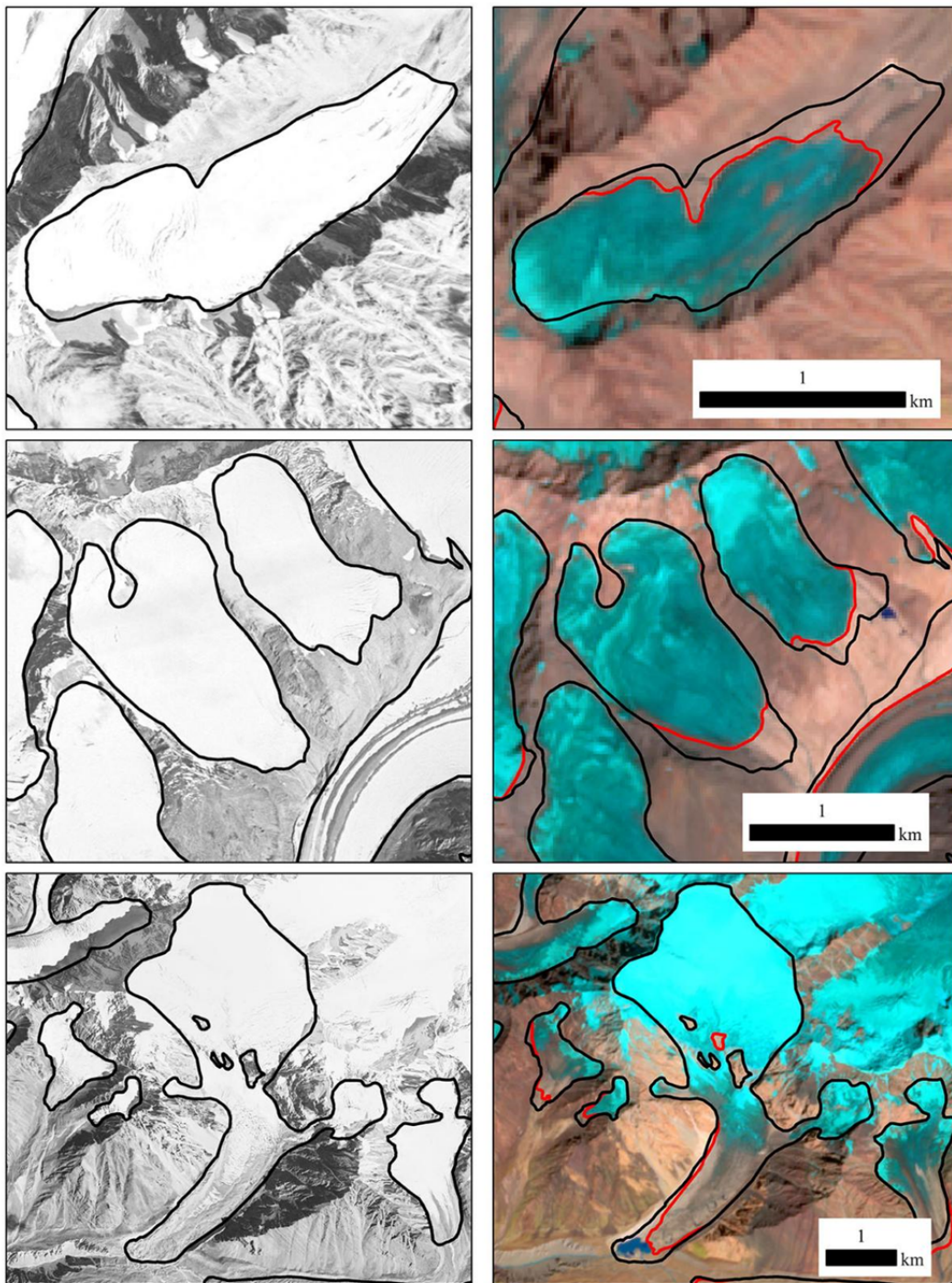
Fig. 3 Manual digitization of glacier outlines from Corona (1971; left panel) and Sentinel 2 (2020; right panel) images. Glacier outlines were adjusted in the lower ablation zone. Upper accumulation shows no visible changes during the study period.

also performed to extract water bodies and emerging snouts (Appendix 7). The semi-automatic techniques produced rapid output with some difficulties regarding differentiation between ice and seasonal snow cover, shaded areas, as well as water bodies (Appendix 8). Extensive manual editing and post-processing was required to exclude misclassified pixels and to produce precise glacier margins, especially in the case of debris-covered glaciers. Due to these difficulties, semi-automatic techniques were rejected in favor of manual mapping. Although time-consuming and sometimes subjective (Bhambri et al.

2011; Paul et al. 2013), manual mapping remains the most appropriate method to extract detailed and reliable information on glaciers (Fig. 3). The latest glacier outlines of 2020 were exported to Google Earth (GE) and further corrected for better visualization and delineation of debris-covered glacier tongues (Das and Sharma 2019). Image enhancement techniques (i.e., gamma stretching, sharpening) and several geometric and topographic features (i.e., river channel emerging from ice, presence of ice cliffs, and proglacial lakes) were used to delineate debris-covered glaciers (Fig. 3).

A glacier inventory was generated using LISS IV (5 m spatial resolution) images from 2013 with a minimum threshold size of >0.02 km² as recommended by the Randolph Glacier Inventory (RGI; Frey et al. 2012). The contiguous ice masses were separated into entities based on the generated watersheds extracted from ASTER GDEM v2 by using the Hydrology Tool in ArcGIS 10.2.2, and further checked and corrected in GE using the 3-D view (Das and Sharma 2019). Each glacier polygon was labeled by corresponding numbers and its topographic parameters (i.e., slope, aspect, elevation), derived in ArcGIS 10.2.2. The hypsometric integral (HI) was computed based on the approach suggested by Jiskoot et al. (2009). Glaciers were grouped into five HI categories: very top-heavy (HI < –1.5), top-heavy (–1.5 < HI < –1.2), equidimensional (–1.2 < HI < 1.2), bottom-heavy (1.2 < HI < 1.5) and very bottom-heavy (HI > 1.5). Top-heavy glaciers are characterized by broad accumulation area, whereas bottom-heavy glaciers have small accumulation zones and long tongues (Jiskoot et al. 2009). The area distribution is strongly skewed towards the top of the elevation range for very top-heavy glaciers and vice-versa for the very bottom-heavy glaciers.

3.3.2 Multi-temporal change analysis

Glacier change detection was carried out for three distinct time spans: 1971–2020, 1971–2000, and 2000–2020. Glacier outlines of 2013 (LISS IV) were used as a baseline and overlaid on multi-temporal satellite images as suggested in previous studies (Bhambri et al. 2011; Chand and Sharma 2015; Das and Sharma 2019). Overlay adjustments were restricted to the lower part as the upper accumulation area exhibits little detectable changes during the observation period (Fig. 3). Due to cloud coverage on the Corona images from 1971, change analysis was restricted to 233 glaciers. The areas of exposed rocks in the upper part of the glaciers were mapped, and the calculated areas were deducted from the total glacier-covered area, considering that the ice was lost from these rock faces. The combined area of glaciers fragmented between 1971 and 2020 was recorded for change detection.

The 233 analyzed glaciers were categorized based on the percentage of their debris-covered area in relation to their total area, and a change analysis was carried out for each class. Glaciers are grouped into six classes: type I (no debris, 0 %), type II (1%–10 %), type III (11%–20%), type IV (21%–30%), type V (31%–40%), and type VI (41%–50%). Simple linear regression analysis was performed to assess the relation between glacier area change as well as terminus retreat and multiple topographic parameters.

3.3.3 Terminus change

Glacier length was represented by the center flow line corresponding to the longest flow distance (Fig. 4). Due to multiple accumulation areas, complex geometry, crevasses and debris-coverage (i.e., Dali, Mayar, and Mulkila glaciers) the delineation of the central flow line was difficult in some cases and high-resolution GE imagery together with field measurements were used as auxiliary data. Glacier length changes were estimated based on two established approaches: (1) along the center flow line (Lopez et al. 2010; Machguth and Huss 2014) and (2) mean length change using 50 m horizontal strip lines (Koblet et al. 2010; Bhambri et al. 2012; Schmidt and Nüsser 2012; Thakuri et al. 2014) (Fig. 4).

3.4 Glacier lake mapping

Glacier lakes were mapped for 1971 (Corona images), 2000 (Landsat data) and 2020 (Sentinel 2 data) in order to analyze their evolution and changes. Glacier lakes were delineated using a standardized semi-automatic approach based on Normalized Difference Water Indices (NDWI = B_{NIR}–B_{Blue}/B_{NIR}+B_{Blue}) (Schmidt et al. 2020) and manually corrected based on visual interpretations. A threshold value of >0.4 was used in order to exclude snow and ice covered areas. Water bodies below 3800 m a.s.l. were deleted because at such altitudes no glacial lakes exist in the study region under given climatic and environmental conditions. The remaining classified water pixels were converted to vector data and
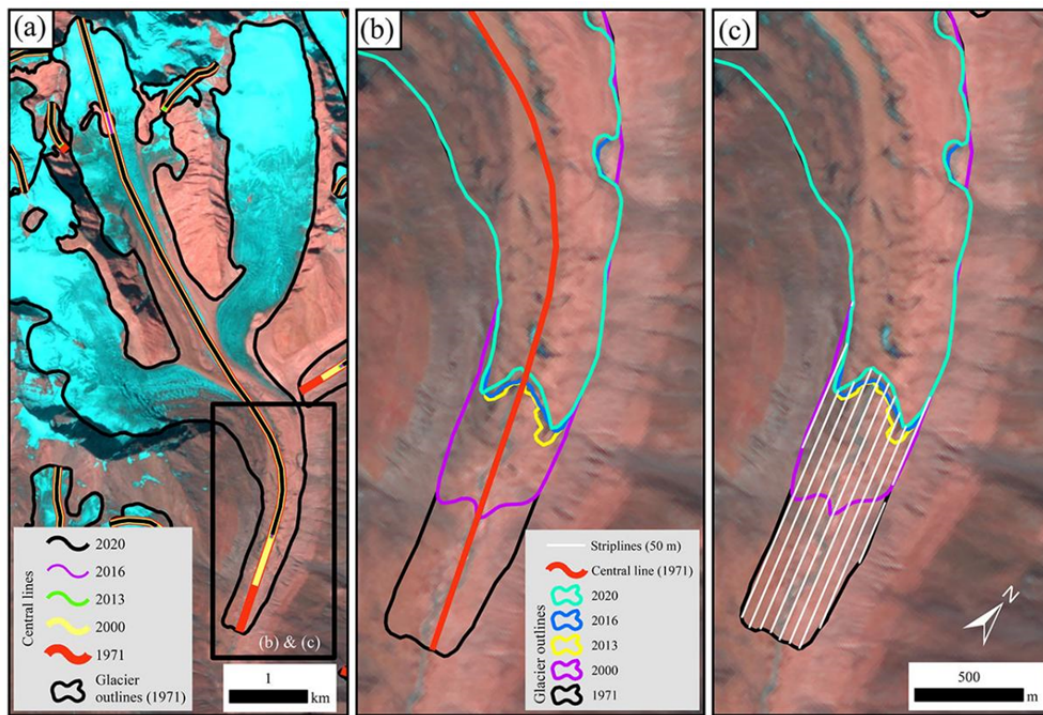
Fig. 4 (a) Example of length measurements based on central flow line of Bagrari Glacier. (b) Length change calculation based on the central line. (c) Length change calculation based on horizontal strip lines. Sentinel 2 image (12-4-3 bands) is shown in the background.

misclassified pixels together with all lakes <0.003 km² were removed (Gardelle et al. 2011; Zhang et al. 2015; Shukla et al. 2018), because such changes were regarded as too uncertain given the spatial resolution (30 m) of Landsat images from 2000. On panchromatic Corona images, the lakes were manually digitized on-screen based on detailed visual interpretation. Following the classification schema of Mergili et al. (2013) and Gardelle et al. (2011) the lakes were categorized into four main classes: supraglacial lake (SGL), pro/periglacial lake in contact with glacier (PGLC), pro/periglacial lakes away from the glacier (PGLA), landslide/moraine-dammed lake (MDL). For the PGLA category, a buffer of 2.5 km from the glacier boundary was applied (Shukla et al. 2018).

3.5 Mapping uncertainty

Measurement accuracy of the glacier area from individual spatial data is limited by sensor resolution (Hall et al. 2003). Potential errors in this study arise through the processes of image registration and digitization, and difficulties in the correct identification of glacierized area (Das and Sharma 2019). The mapping uncertainty was estimated by calculating a buffer around each glacier (Hall et al. 2003; Bolch et al. 2010). The buffer size was chosen based on the estimated shift caused by the misregistration of images in relation to the base image and pixel size (Appendix 9). According to the standard error propagation, the area change uncertainty was estimated as the root sum square of the uncertainty for glacier outlines mapped from different sources (Das and Sharma 2019). The final mapping uncertainty was calculated at ~1.14%, ~2.81%, ~0.98%, and ~1.96% for Corona, Landsat pan-sharpened ETM+, LISS IV, and Sentinel 2 images, respectively. The resultant uncertainties are within the range reported in previous studies (Bolch et al. 2010; Bhambri et al. 2011; Das and Sharma 2019). Terminus change uncertainty ($U_{Terminus}$) was calculated for multi-temporal images using the following equation based on Hall et al. (2003):

$$U_{Terminus} = \sqrt{[(a)^2 + (b)^2]} + REG_{Error} \qquad (1)$$

where a is the pixel resolution of imagery 1, b is the pixel resolution of imagery 2, and REG_{ERROR} is the registration error to the base image. Hence, the uncertainty can be calculated in the case of the 1971 Corona image as follows:

$$U_{Terminus} = \sqrt{[(2)^2 + (10)^2]} + 5.71 = 15.9 \text{ m} \qquad (2)$$

307

The calculated uncertainty was 28.5 m for Landsat pan-sharpened ETM+ (2000), 12.9 m for LISS 4 (2013), 16.8 m for Sentinel 2B (2018), and 16.2 m for Sentinel 2B (2020) image. Uncertainty in the glacial lake area was estimated to be half a pixel (Schmidt et al. 2020).

3.6 Climatic trend analysis

In order to investigate long-term trends in climatic parameters (temperature and precipitation) and to explain glacier changes, the following gridded temperature and precipitation datasets were used: (i) gridded precipitation and temperature data (1900–2017) available from the University of Delaware (UD) at 0.5° spatial grid (Legates and Willmott 1990), (ii) National Centers for Environmental Prediction and the National Center for Atmospheric Research (NCEP/NCAR) temperature and precipitation data (1948–2018) for grid point 32.5°N and 77.5°E available at a spatial resolution of 2.5° (Kalnay et al. 1996), (iii) APHRODITE temperature (1961–2007) and precipitation (1951–2007) available at 0.5° spatial resolution (Yatagai et al. 2012). NCEP/NCAR and the UD datasets are available at mean monthly averages. APHRODITE datasets are based on in situ observation and available at daily averages. Decadal trend analysis was performed for climatic data in accordance with glacier change measurements. Temperature and precipitation trends were evaluated based on Mann–Kendall method. To analyze the long-term decadal trend in temperature and precipitation, the entire observation period was categorized into three time-spans: 1900–1950, 1950–1990, and 1990–2018. Climatic trend break points were chosen based on manual visualization using line plots. Additionally, the break point was analyzed based on the "At Most One Change" method using the Change Point Analysis tool in Origin pro software (Appendix 10).

4 Results

4.1 Glacier characteristics

306 glaciers (>0.02 km²) cover an area of 360.3 ± 3.9 km² in the Bhaga basin in 2013 (Table 3). Out of all mapped glaciers, 186 glaciers (61%) are smaller than 0.5 km², covering an area of only 33.6 km² (9% of the total ice area). One-third belongs to the size classes 0.5–1 km² and 1–5 km², which comprise 40% of the total glacierized area, and only ~2% are larger than 10 km² and cover nearly 30 % of the total glacierized area (Fig. 5a). The mean length of glaciers amounts to 1.7 km, while most glaciers (177) are shorter than 2 km (Fig. 5c). The longest glaciers are Milang and Mulkila with a length of 15.1 km and 14.2 km, respectively.

The number and area of glaciers vary significantly between different watersheds. Most glaciers (153) are located in the JCW with a total area of 186.4 ± 2.1 km² (52% of the glacierized area of Bhaga basin), whereas the BUW contains the smallest glacierized area with 37.2 ± 0.4 km² (~10% of the total glacierized area). The MV comprises the smallest number of glaciers (30), but they cover an area of 85.9 ±1 km² which amounts to 24% of the total glacierized area. Two of the largest glaciers (Mulkila and Milang) are located in this watershed accounting for 13 % of the total glacier-covered area.

Table 3 Glacier characteristics in the Bhaga basin and sub-watersheds based on LISS 4 (2013) and ASTER GDEM analysis.

Parameters	Bhaga basin	Bhaga Lower	Jankar Chhu	Bhaga Upper	Milang Valley
a) Region-wide averages					
No of glaciers	306	42	153	58	53
Glacierized area (km²)	360.3 ± 4.0	50.6 ± 0.5	186.4 ± 2.1	37.2 ± 0.4	85.9 ± 1.0
Number of debris cover tongues	140	15	81	21	23
Debris cover area (km²)	55.8 ± 0.6	6.2 ± 0.1	19.6 ± 0.2	8.8 ± 0.1	21.1 ± 0.3
Debris cover (% total area)	15.5	12.3	10.5	23.7	24.6
b) Glacier averages					
Minimum elevation (m a.s.l)	5071	4824	5171	5108	4938
Median elevation (m a.s.l)	5292	5129	5369	5291	5200
Maximum elevation (m a.s.l)	5529	5426	5597	5498	5451
Slope (degree)	24.2	23.5	24.3	23.1	26.4
Majority Aspect	NE-NW	W	NE-NW	NE	W
Size (km²)	1.2	1.2	1.2	0.6	1.6
Length (km)	1.7	2	1.6	1.5	1.9
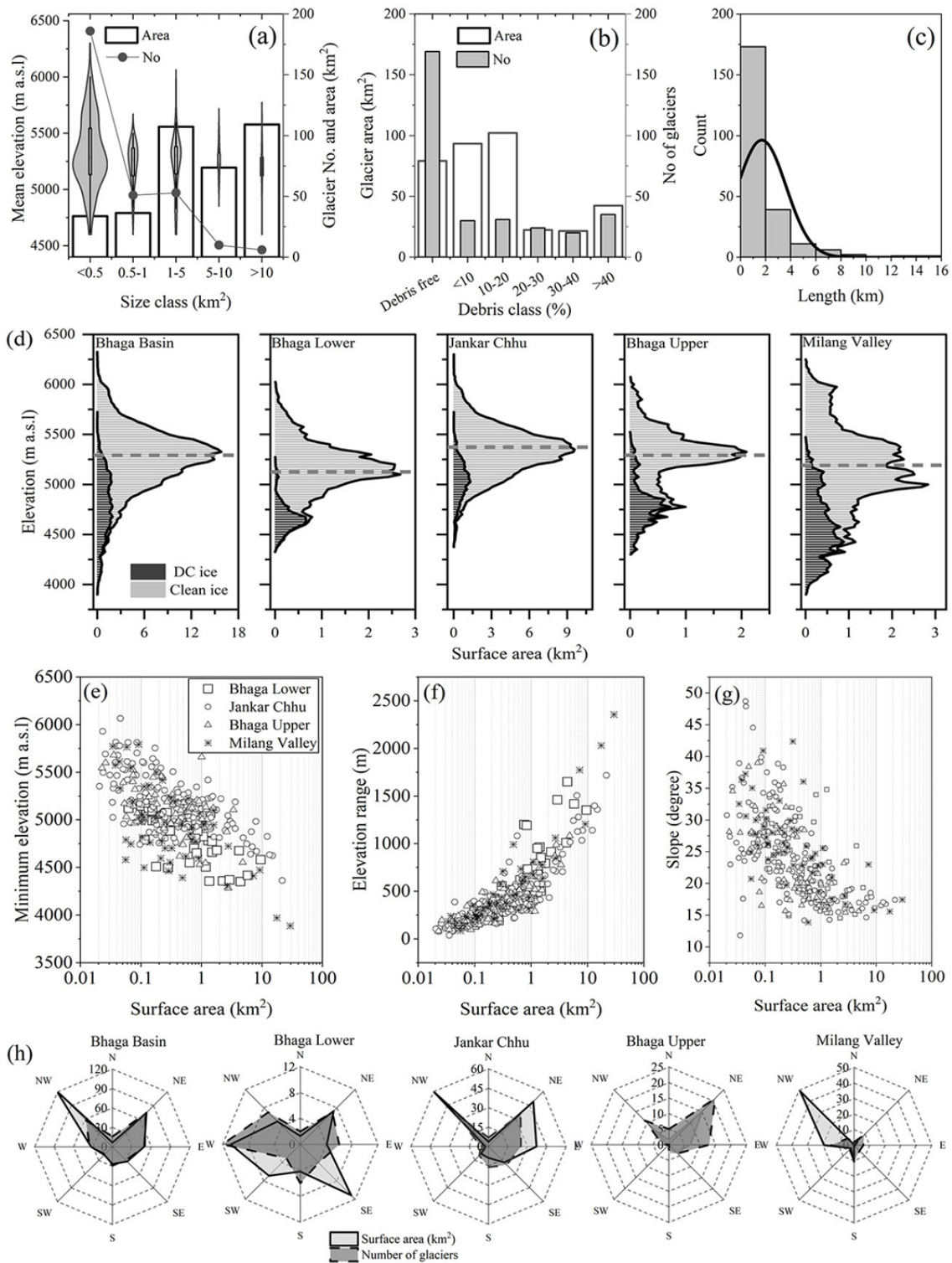
Fig. 5 Glacier distributions with respect to various parameters for the Bhaga basin. (a) Size class distribution with respect to the number, total area, and mean elevation of glaciers. (b) Glacier distribution based on the debris class. (c) Frequency distribution based on length for 233 analyzed glaciers. (d) Elevation-dependent ice distribution for the entire Bhaga basin and its tributary watersheds. The dotted grey line represents the mean elevation of the studied glaciers. Scatter plots of surface area with respect to the (e) minimum elevation, (f) elevation range, and (g) slope categorized based on watersheds. (h) Distribution of glaciers according to aspects in the Bhaga basins and its tributary watersheds. Glacier area, elevation, and orientations were derived from LISS IV (23 Oct 2013) and ASTER GDEM v2.

140 glaciers are debris-covered with a total area of 55.7 ± 0.6 km² (15% of the total glacierized area). 61 glaciers belong to the two debris classes 1%–10% and 11%–20% (Fig. 5b). The percentage of debris-covered ice areas varies between watersheds. While the JCW contains the smallest percentage of debris-covered glacier areas (10%), nearly 25% of the glacierized area in the BUW and MV is debris-covered (Table 3; Appendix 11).

The mean altitude of glaciers in the Bhaga basin ranges from about 5070 to 5530 m a.s.l., with an average of about 5300 m a.s.l. (Table 3). Higher heterogeneity in elevation-dependent ice distribution is visible in the MV (Fig. 5d). Minimum elevation and elevation range show a clear relation with glacier size, with the largest glaciers reaching down to 3820 m a.s.l. (Fig. 5e, f). In general, larger glaciers (>5 km²) with extensive accumulation areas can reach further down than smaller ones. The average slope of all glaciers in the Bhaga basin amounts to 24° (Fig. 5g). With increasing glacier size, the mean slope angle

decreases. Most glaciers are oriented towards northern directions (NW, N, NE) (Table 3), although heterogeneity can be observed between watersheds (Fig. 5h). Glaciers in the BLW are located mainly on west- and southeast-facing slopes, whereas most glaciers in the MV are on northwest- and north-facing slopes.

4.2 Multi-temporal glacier changes

4.2.1 Entire Bhaga basin

The glacierized area decreased from 362.9 ± 4.0 km² in 1971 to 332.7 ± 3.6 km² in 2020, a decrease of 8.3 ± 1.5% (0.17 ± 0.03 % yr⁻¹). Due to fragmentation, the number of analyzed glaciers increased from 233 to 242 (Table 4, Fig. 6). The area loss of individual glaciers varied widely from 1.7% to 65.9% (Appendix 12). The mean annual area change rate in recent decades (2000–2020) has almost doubled (0.21 % yr⁻¹) compared to 1971–2000 (0.14 % yr⁻¹). During the observation period, clean ice area decreased from
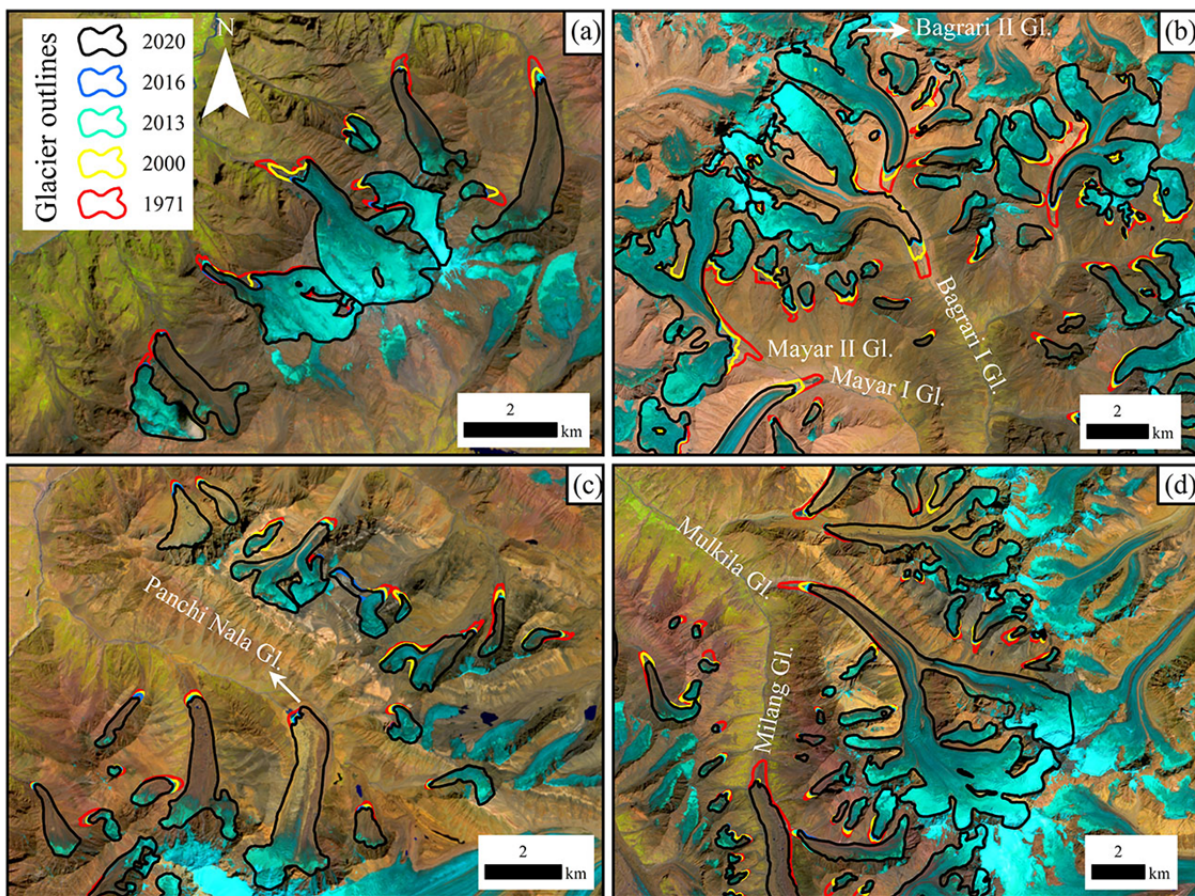
Fig. 6 Examples of glacier changes in the Bhaga basin: a) part of Bhaga lower watersheds, b) part of the Jankar Chhu watershed, c) part of the Bhaga lower watershed, and d) part of the Milang valley. False-color composite from Sentinel 2B image (9-3-2 bands) is used as background.

Table 4 A decadal glacier change rate in the Bhaga basin and its tributary watersheds from 1971 to 2020 based on remote sensing.

Watersheds	Year	Ice extent (km²)		Period	Surface area change		
		No	Total		Change (Km²)	Change (%)	Change (% yr⁻¹)
(a) Entire Bhaga Basin	1971	233	362.9 ± 4.0	1971-2020	-30.2 ± 5.4	-8.2 ± 1.5	-0.2 ± 0.1
	2000	233	347.4 ± 3.8	1971-2000	-15.5 ± 5.3	-4.3 ± 0.1	-0.2 ± 0.1
	2013	242	336.8 ± 3.7	2000-2013	-10.5 ± 5.2	-3.0 ± 0.1	-0.2 ± 0.1
	2016	242	335.4 ± 3.7	2013-2016	-1.4 ± 5.2	-0.4 ± 0.1	-0.1 ± 0.1
	2018	242	334.1 ± 3.7	2016-2018	-1.3 ± 4.2	-0.4 ± 0.1	-0.2 ± 0.1
	2020	242	332.7 ± 3.6	2018-2020	-1.4 ± 4.0	-0.4 ± 0.1	-0.2 ± 0.1
(b) Bhaga Lower Watershed	1971	26	43.4 ± 0.5	1971-2020	-4.6 ± 0.6	-10.6 ± 1.4	-0.2 ± 0.1
	2000	27	40.9 ± 0.5	1971-2000	-2.4 ± 0.6	-5.5 ± 1.0	-0.2 ± 0.1
	2013	28	39.4 ± 0.4	2000-2013	-1.5 ± 0.6	-3.8 ± 1.0	-0.3 ± 0.1
	2016	28	39.2 ± 0.4	2013-2016	-0.2 ± 0.6	-0.6 ± 1.0	-0.2 ±0.1
	2018	28	39.0 ± 0.4	2016-2018	-0.2 ± 0.6	-0.5 ± 1.0	-0.2 ± 0.1
	2020	28	38.8 ± 0.4	2018-2020	-0.2 ± 0.6	-0.5 ± 1.0	-0.3 ± 0.1
(c) Jankar Chhu watershed	1971	127	196.2 ± 2.2	1971-2020	-15.8 ± 2.9	-8.1 ± 1.5	-0.2 ± 0.1
	2000	127	188.5 ± 2.1	1971-2000	-7.7 ± 2.9	-3.9 ± 1.1	-0.1 ± 0.1
	2013	131	182.2 ± 2.0	2000-2013	-6.3 ± 2.9	-3.4 ± 0.9	-0.3 ± 0.1
	2016	131	181.5 ± 2.0	2013-2016	-0.8 ± 2.9	-0.4 ± 0.5	-0.3 ± 0.1
	2018	131	180.7 ± 2.0	2016-2018	-0.7 ± 2.9	-0.4 ± 0.5	-0.2 ± 0.1
	2020	131	180.4 ± 2.0	2018-2020	-0.3 ± 1.5	-0.2 ± 0.3	-0.1 ± 0.1
(d) Bhaga Upper Watershed	1971	36	34.1 ± 0.4	1971-2020	-4.6 ± 0.5	-13.5 ± 1.7	-0.3 ± 0.1
	2000	37	31.8 ± 0.4	1971-2000	-2.3 ± 0.5	-6.9 ± 1.5	-0.2 ± 0.1
	2013	38	30.3 ± 0.3	2000-2013	-1.5 ± 0.5	-4.6 ± 1.2	-0.4 ± 0.1
	2016	38	30.1 ± 0.3	2013-2016	-0.3 ± 0.5	-0.8 ± 1.0	-0.3 ± 0.1
	2018	38	29.9 ± 0.3	2016-2018	-0.2 ± 0.5	-0.6 ± 1.0	-0.3 ± 0.1
	2020	38	29.5 ± 0.3	2018-2020	-0.4 ± 0.8	-1.2 ± 1.0	-0.6 ± 0.1
(e) Milang Valley	1971	44	89.1 ± 1.0	1971-2020	-4.9 ± 1.3	-5.4 ± 1.6	-0.1 ± 0.1
	2000	45	86.1 ± 0.9	1971-2000	-3.1 ± 1.3	-3.6 ± 1.2	-0.1 ± 0.1
	2013	45	84.8 ± 0.9	2000-2013	-1.2 ± 1.3	-1.4 ± 1.0	-0.1 ± 0.1
	2016	45	84.7 ± 0.9	2013-2016	-0.2 ± 1.3	-0.2 ± 0.1	-0.1 ± 0.1
	2018	45	84.5 ± 0.9	2016-2018	-0.2 ± 1.3	-0.2 ± 0.1	-0.1 ± 0.1
	2020	45	84.2 ± 0.8	2018-2020	-0.3 ± 1.5	-0.4 ± 0.2	-0.2 ± 0.1

318.3 ± 3.5 km² (1971) to 275.1 ± 3.0 km² (2020), a relative decrease of 13.5 ± 1.2 %, while the debris-covered ice area increased by 13.2 ± 0.7 km² (31.1 ± 1.6 %) (Appendix 13).

4.2.2 Bhaga lower watershed (BLW)

The glacierized area in the BLW decreased from 43.4 ± 0.5 km² (1971) to 38.8 ± 0.4 km² (2020), a loss of 4.4 ± 0.6 km² (10.6 ± 1.4 % or 0.21 ± 0.03 % yr⁻¹). Due to fragmentation, the number of glaciers increased from 26 (1971) to 28 (2020) (Table 4). From 1971–2000, the mean annual surface area loss rate was ~0.19 ± 0.01 % yr⁻¹, which has increased to ~0.29 ± 0.03 % yr⁻¹ since 2000 (Table 4). Clean ice area decreased from 37.3 ± 0.4 km² in 1971 to 32.8 ± 0.4 km² in 2020, a loss of 4.5 ± 0.5 km² (12.1 ± 1.4 %) and debris-covered glacier area slightly increased by 1.6 ± 0.1 %, the lowest rate between the four watersheds (Appendix 13).

4.2.3 Jankar Chhu watershed (JCW)

In the JCW the glacier area decreased from 196.2

± 2.2 km² (1971) to 180.4 ± 2.0 km² (2020), a loss of 15.5 ± 2.9 km² (8.0 ± 1.5 % or 0.16 ± 0.01 % yr⁻¹) (Table 4). From 2000 to 2020, glaciers showed higher mean annual area loss (0.21 ± 0.01 % yr⁻¹) compared to 1971−2000 (0.13 ± 0.01% yr⁻¹). The clean ice area decreased by 23.8 ± 2.6 km² (13.1 ± 2.1 %), while debris-covered area increased by 8.4 ± 0.2 km² (65.1 ± 2.4 %) between 1971 and 2020 (Appendix 13). Four large valley type glaciers were studied in detail (Table 5). The two largest glaciers Dali and Mayar I are characterized by a below average decreasing rate of 0.03 ± 0.01 % yr⁻¹ and 0.05 ± 0.01 % yr⁻¹, respectively; whereas, the decreasing rate of Mayar II Glacier is above-average (0.21 ± 0.03 % yr⁻¹).

4.2.4 Bhaga upper watershed (BUW)

In the BUW the glacierized area decreased from 34.1 ± 0.4 km² (1971) to 29.5 ± 0.3 km² (2020), a loss of 4.2 ± 0.5 km² (12.5 ± 1.7 %), which is the highest mean annual deglaciation rate of 0.27 ± 0.03 % yr⁻¹ in all four watersheds. Furthermore, the mean annual deglaciation rate in the period 2000−2020 was much

Table 5 (a) Surface area, total change, and mean annual change; (b) glacier lengths and their changes (absolute, mean annual) for selected glaciers in the Bhaga basin between 1971 (Corona KH) and 2020 (Sentinel 2). For location of the glaciers in the Bhaga basin see Fig. 1b.

(a) Surface area					
Glaciers	Covered area (km²)		Estimated change in area		Mean annual change in area
	1971	2020	(km²)	(%)	(% yr⁻¹)
Dali	22.0 ± 0.2	21.7 ± 0.2	-0.3 ± 0.2	-1.3 ± 0.1	-0.1 ± 0.1
Mayar I	15.3 ± 0.2	14.9 ± 0.2	-0.4 ± 0.2	-2.6 ± 0.1	-0.1 ± 0.1
Mayar II	15.0 ± 0.2	13.5 ± 0.1	-1.5 ± 0.2	-10.2 ± 0.1	-0.2 ± 0.1
Bagrari I	14.1 ± 0.2	13.3 ± 0.1	-0.8 ± 0.1	-5.4 ± 0.1	-0.1 ± 0.1
Panchi Nala	4.9 ± 0.1	4.8 ± 0.1	-0.1 ± 0.1	-1.8 ± 0.1	-0.1 ± 0.1
Mulkila	29.7 ± 0.3	29.3 ± 0.3	-0.3 ± 0.2	-1.2 ± 0.1	-0.1 ± 0.1
Milang	21.1 ± 0.2	20.2 ± 0.2	-0.9 ± 0.1	-4.1 ± 0.1	-0.1 ± 0.1
(b) Terminus retreat					
Glaciers	Length along central line (m)		Terminus change		
	1971	2020	(m)	(m yr⁻¹)	Strip lines (m yr⁻¹)
Dali	8297.8 ± 15.9	7709.5 ± 15.9	-588.3 ± 15.9	-12.3 ± 0.5	-11.2 ± 0.5
Mayar I	10176.6 ± 15.9	9223.5 ± 15.9	-953.2 ±15.9	-19.9 ± 0.5	-20.5 ± 0.5
Mayar II	8296.1 ± 15.9	7201.6 ± 15.9	-1094.6 ± 15.9	-22.8 ± 0.5	-15.5 ± 0.5
Bagrari I	8543.6 ± 15.9	6939.8 ± 15.9	-1603.9 ± 15.9	-33.4 ± 0.5	-25.3 ± 0.5
Panchi Nala	5035.5 ± 15.9	4816.9 ± 15.9	-218.6 ± 15.9	-4.6 ± 0.5	-4.6 ± 0.5
Mulkila	14219.3 ± 15.9	13043.9 ± 15.9	-1175.4 ± 15.9	-24.5 ± 0.5	-21.1 ± 0.5
Milang	15051.8 ± 15.9	14148.1 ± 15.9	-903.7 ± 15.9	-18.8 ± 0.5	-10.1 ± 0.5

higher (0.36 ± 0.09 % yr⁻¹) than 1971–2000 (~0.24 ± 0.05 % yr⁻¹). The recession rate has increased in subsequent years (Table 4). Between 1971 and 2020, clean ice area decreased by 6.9 ± 0.3 km² (25.1 ± 2.6 %) while debris-covered area increased by 2.3 ± 0.1 km² (32.4 ± 1.2 % or 0.68 ± 0.1 % yr⁻¹) (Appendix 13).

4.2.5 Milang valley (MV)

The glaciers of the MV decreased from 89.1 ± 1.0 km² to 84.2 ± 0.9 km² between 1971 and 2020, a loss of 4.9 ± 1.3 km², the lowest recession rate (5.4 ± 1.6 %, 0.11 ± 0.03 % yr⁻¹) in all four watersheds (Table 4). Clean ice area decreased by 8.8 ± 0.9 km² (11.0 ± 1.5 % or 0.24 ± 0.01 % yr⁻¹) while debris-covered area increased by 3.6 ± 0.1 km² (15.9 ± 1.2 % or 0.33 ± 0.02 % yr⁻¹) between 1971 and 2020 (Appendix 13).

### 4.2.6 Topography related changes and correlation

An inverse relationship between glacier size and percentage area loss was observed in the entire Bhaga basin; the relative ice loss decreased with increasing glacier size (Fig. 7a). Glaciers of the size classes <0.5 km² and 0.5–1 km² experienced a higher relative loss of 25 % (0.5 % yr⁻¹) and 13 % (0.3 % yr⁻¹), respectively compared to glaciers of the size classes 5–10 km² and >10 km², which show the lowest relative loss of 6.8 % (0.1 % yr⁻¹) and 3.8 % (0.1 % yr⁻¹), respectively between 1971 and 2020. Glacier size and relative surface area change correlate negatively ($r = -0.3$),

while the absolute area change showed a significant positive correlation ($r = 0.7$) with glacier size by simple linear regression (Fig. 8). Area change decreases as debris cover increases (Appendixes 14 and 15). For glaciers with 31–40 % (Type V) and 41–50 % (Type VI) debris cover, the lowest area loss of 1.58 km² (7.2%; ~0.1 % yr⁻¹) and 3.54 km² (7.1%; ~0.1 % yr⁻¹), respectively, was observed (Appendix 15). In contrast, the surface area of debris-free glaciers (Type I; 1%–10%) decreased from 53.61 ± 1.5 km² (1971) to 45.27 ± 1.4 km² (2020), a loss of 8.3 ± 0.9 km² (15.6 %; 0.3 % yr⁻¹).

The elevation-dependent glacier loss analysis (Fig. 7b; Appendix 15) shows that absolute area loss was higher (22.9 ± 0.4 km²) for glaciers terminating <5400 m a.s.l. compared to those terminating >5400 m a.s.l. (5.8 ± 0.2 km²). But relative area change was higher for glaciers located >5400 m a.s.l. (18.6 % or 0.38 % yr⁻¹) than those reaching down to 5000 m a.s.l. (7.8 % or 0.16 % yr⁻¹) between 1971 and 2020 (Fig. 7b; Appendix 15). A significant negative correlation ($r= -0.5$) between minimum elevation and glacier change was observed, indicating that higher decreasing rates can be observed at low than at high altitude glaciers. The maximum elevation and elevation range show significant positive relations with glacier change ($r= 0.3$ and $r= 0.6$, resp.) indicating that elevation range is more influential for glacier change than other elevation parameters (Fig. 8). The analysis of hypsometric characteristics in the Bhaga basin indicates
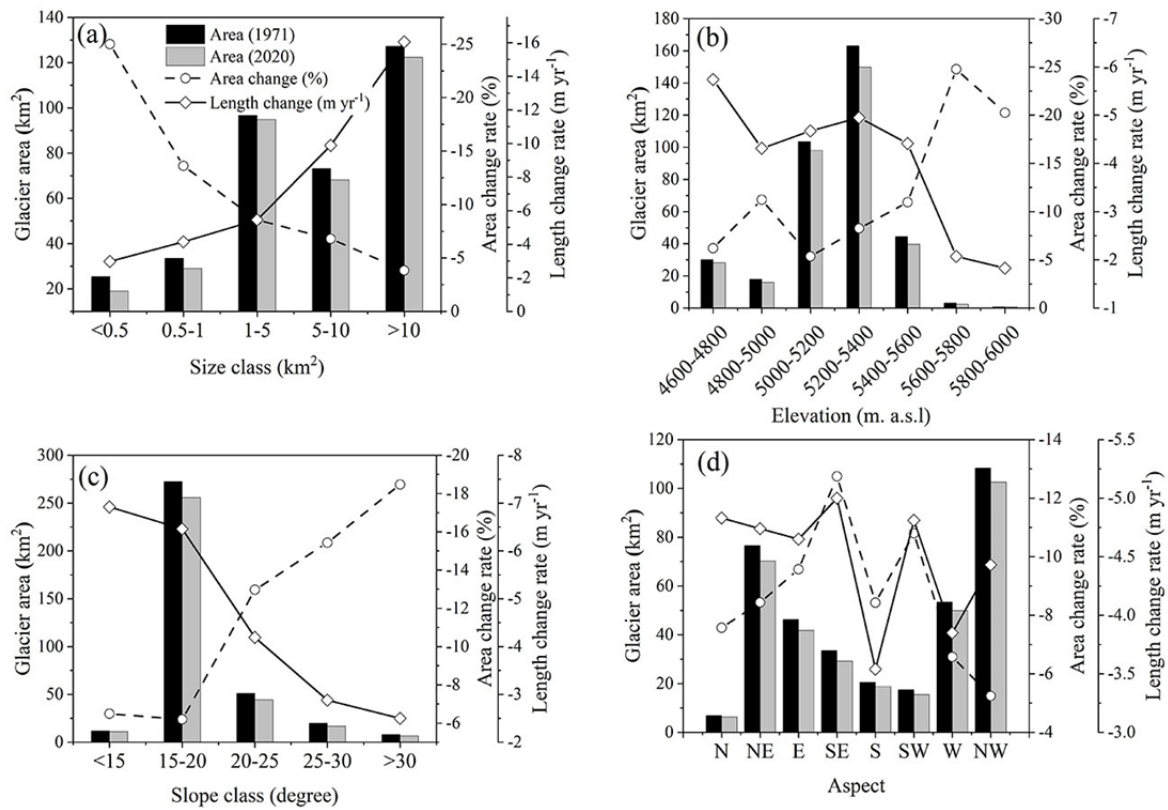
Fig. 7 Glacier changes based on (a) Size class, (b) elevation, (c) slope, and (d) aspects in the Bhaga basin. Surface area was derived from Corona (1971) and Sentinel 2B (2020) images.
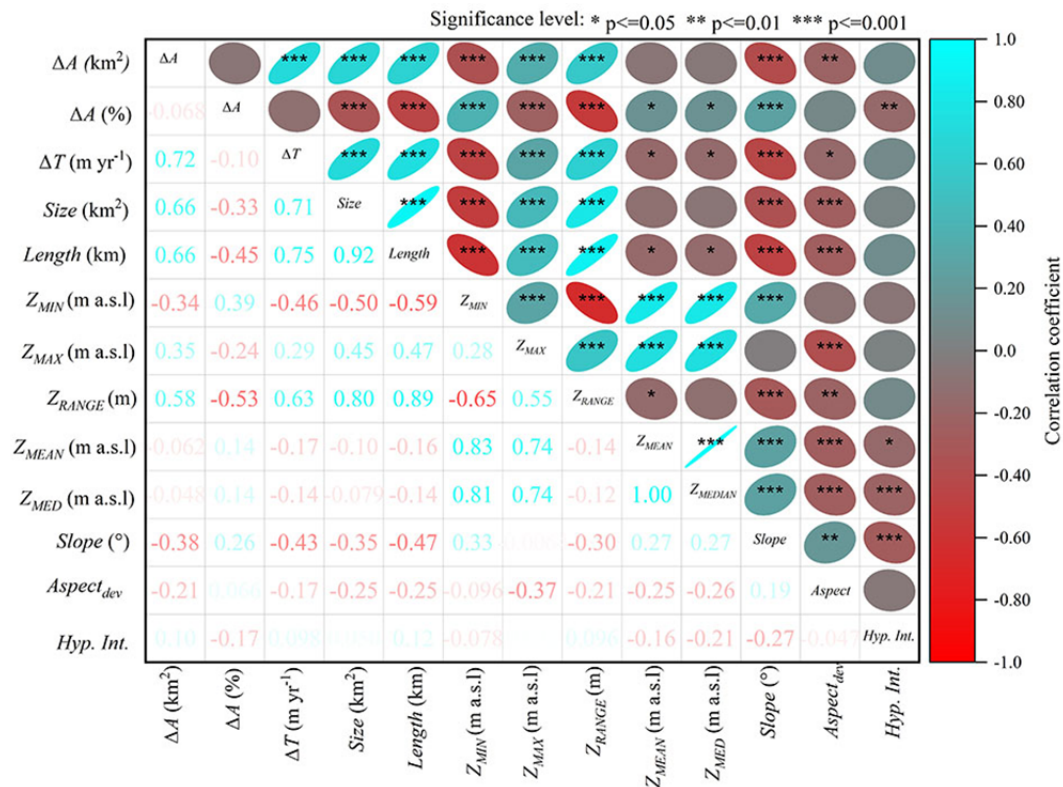
Fig. 8 Correlation plots between glacier change indicators and topographic parameters.

that relative area change was higher (0.24 ± 0.01 % yr⁻¹) for glaciers with top-heavy than bottom-heavy geometries (0.16 ± 0.01 % yr⁻¹). (Appendix 15).

Slope-dependent ice loss revealed that the area change rate of glaciers having a mean slope >30° is nearly three times higher (18.5 % or 0.38 % yr⁻¹) than those having an average slope of <15° (6.5 % or 0.14 % yr⁻¹) (Fig. 7c). Terminus retreat was larger for gentle-sloped glaciers (<15°; 7.5 m yr⁻¹) and smaller for steep glaciers (>30°; 2.8 m yr⁻¹). Absolute area change is positively correlated (r= 0.4) with surface slope, while relative area loss shows negative relation (r= −0.3). Taking into account the aspect, southward-facing glaciers (SE, S, SW combined) decreased by 10.7 % (0.2 % yr⁻¹), while northward-facing glaciers (NW, N, NE combined) experienced an ice loss of 7 % (0.15 % yr-1) between 1971 and 2020 (Fig. 7d; Appendix 15). The highest area loss was observed for southeast-facing glaciers (12.7 %; 0.3 % yr⁻¹) (Fig. 7d; Appendix 15).

4.3 Frontal retreat

The mean length decrease of the 233 analyzed glaciers amounted to 214.2 ± 15.2 m (4.16 ± 0.5 m yr⁻¹)

between 1971 and 2020. The highest average terminus retreat rate (5.3 ± 0.5 m yr⁻¹) was observed in the BLW, while the lowest retreat rate (4.1 ± 0.5 m yr⁻¹) in the BUW. The mean retreating rate amounted to 15.8 m yr⁻¹ for glaciers >10 km² and 4.2 m yr⁻¹ for glaciers < 1 km² (Fig. 7a). Glaciers terminating below 4800 m a.s.l. are characterized by a higher retreat rate (5.8 m yr⁻¹) than those above 5600 m a.s.l. (2.1 m yr⁻¹) (Fig. 7b). Slope dependent length change rate of glaciers having a mean slope <15° is nearly three times higher (7.5 m yr⁻¹) than those with an average slope of >30° (2.8 m yr⁻¹) (Fig. 7c). Furthermore, terminus retreat rates of north-facing glaciers are slightly smaller (4.6 m yr⁻¹) than south-facing ones (5.5 m yr⁻¹) (Fig. 7d).

A heterogeneous pattern of terminus retreat is shown by large valley glaciers (Table 5; Fig. 9). The largest retreat rates (1604 ± 15.9 m, 25.3 ± 0.5 m yr⁻¹) were observed for Bagrari I glacier in the JCW and the Mulkila glacier (1175 ± 15.9 m, 21.1 ± 0.5 m yr⁻¹) in the MV. The smallest retreats (218 ± 15.9 m, 4.6 ± 0.5 m yr⁻¹) were detected for the heavily debris-covered Panchi Nala glacier in the BUW and Milang glacier (903 ± 15.9 m, 10.1 ± 0.5 m yr⁻¹) in the MV (Table 5).
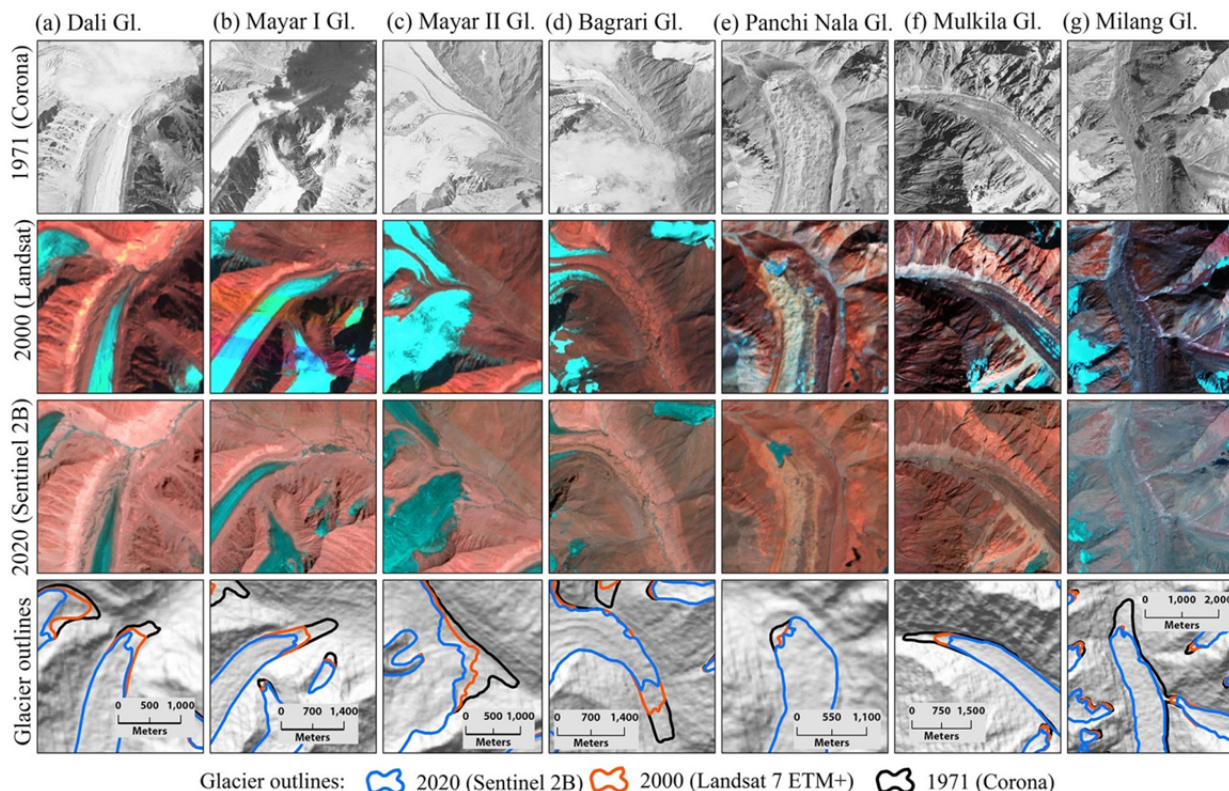

Fig. 9 An example of frontal retreat of seven selected glaciers in the Bhaga basin during 1971−2020.

In general, terminus retreat rate is larger (5.1 m yr⁻¹) for glaciers with bottom-heavy than top-heavy geometries (3.4 m yr⁻¹).

4.4 Glacier lake dynamics

A total of 81 glacial lakes covering an area of 0.93 ± 0.1 km² were mapped in 2020: 22 supraglacial lakes (SGL), 19 proglacial lakes in contact with glacier (PGLC), 35 proglacial lakes away from the glacier (PGLA), and five landslide/moraine-dammed lakes (LML) (Fig. 10). The mean size of all lakes (>0.003 km²) amounts to 0.012 km². The largest glacial lake with a size of 0.1 km² is located in front of the Panchi
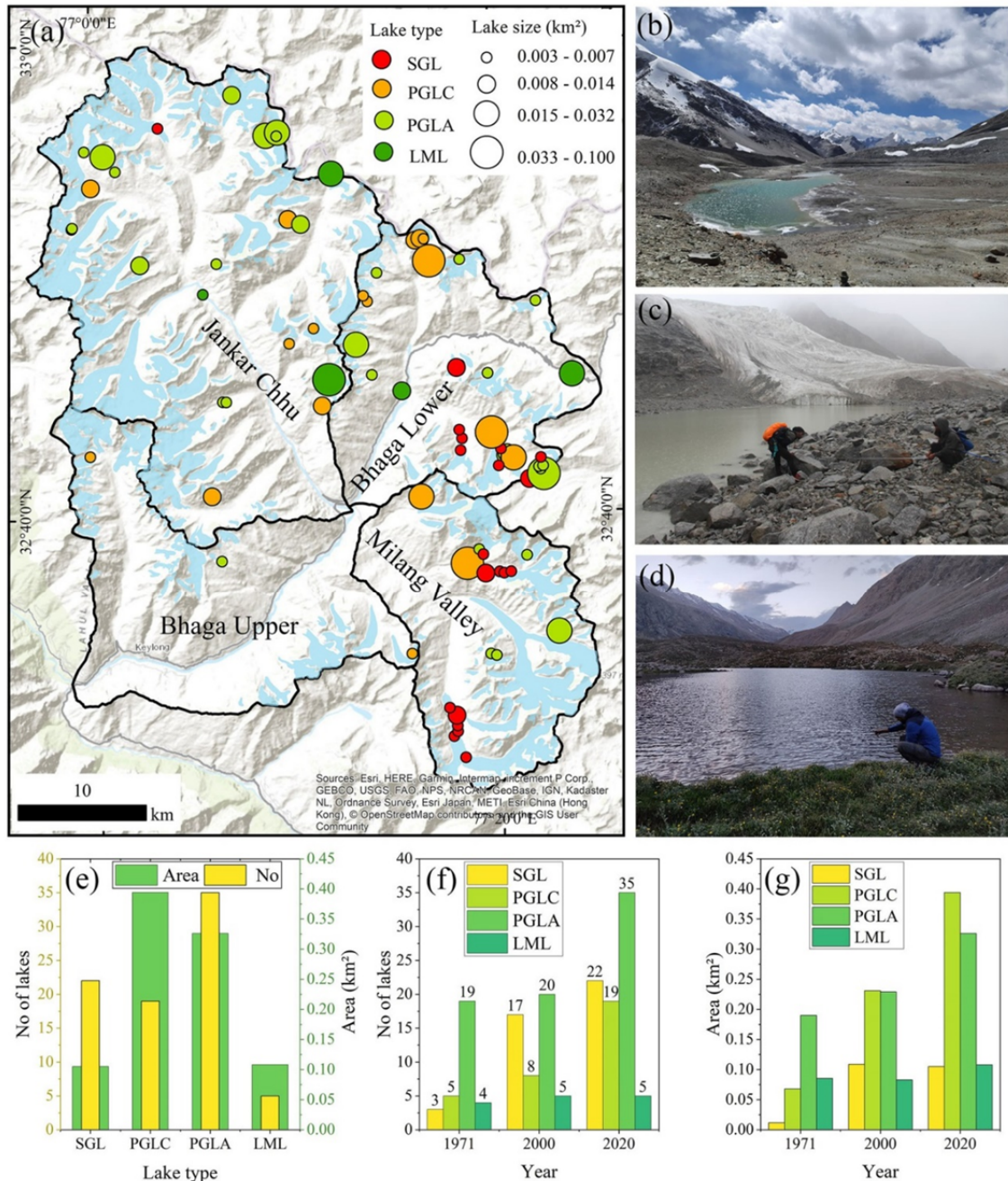
Fig. 10 Evolution and dynamics of glacial lakes in the Bhaga basin. (a) Distribution of glacial lakes in 2020. (b) Field photograph of pro/periglacial lakes away from the glacier (PGLA) near Shingo La. (c) Field photograph of pro/periglacial lake in contact with glacier (PGLC) lake at Mayar II Glacier. (d) Field photograph of landslide/moraine-dammed lake (LML). (e) Statistic of glacial lakes in 2020. (f) Temporal changes in lake number. (g) Changes in lake area between 1971 and 2020. Supraglacial lake (SGL).

Nala glacier in the BUW. The total area of all proglacial lakes (PGLC and PGLA) amounts to 0.72 ± 0.1 km² (77 % of total lake area), while all SGL and LML cover an area of 0.21 ± 0.1 km². Most lakes (33) are located in the BUW with a total area of 0.44 ± 0.1 km² (47% of all lakes), whereas only three lakes exist in the BLW.

Between 1971 and 2020, the number of lakes was more than doubled from 31 to 81, and their total area was almost tripled from 0.35 ± 0.1 km² to 0.93 ± 0.2 km² (0.015 km² yr⁻¹). Considering the various lake categories, many new SGL and PGLC were formed, which number increased from 3 to 22 and from 5 to 19, respectively (Fig. 10c).

4.5 Climatic trends

The used climatic data show varying increasing trends of temperature and decreasing trends of precipitation. Based on UD data, mean annual temperature (MAT) rose by 0.2°C between 1900 and 2017 (Fig. 11a), NCEP/NCAR data show an increase of 0.7°C from 1948–2018 (Fig. 11b; Appendix 16), and APHRODITE data indicated a total increase of 1.2°C from 1961–2015 (Fig. 11c). From 1948–1990 both UD and NCEP/NCAR showed a declining trend of

temperature and precipitation (Fig. 11a-c) and from 1990–2018 an increasing trend of MAT and mean annual precipitation (MAP), which amounts to 0.4°C and 12.8 mm for UD and 2.3°C and 7.6 mm for NCEP/NCAR (Appendixes 16 and 17). In contrast, APHRODITE data indicated a 0.5°C increase of MAT and a MAP decrease by 33.5 mm from 1990–2015 (Fig. 11c). Thus, a drastic upward shift in temperature trend and a downward shift in precipitation can be assumed for the Bhaga basin since 1990. All three datasets indicate an increase in MAT since the beginning of the 21ˢᵗ century (Fig. 11a-c). An overall decreasing trend in precipitation was observed for NCEP/NCAR and APHRODITE datasets, but UD data showed an insignificant increasing trend during the observation period (Fig. 11d-f; Appendix 17).

5   Discussion

5.1   An   updated   and   improved   glacier inventory

The Bhaga basin glacier inventory based on high spatial resolution LISS IV images of 2013 contains 306 glaciers (>0.02 km²), totaling an area of 360.26 ± 3.94 km² (Table 6). The comparison to other
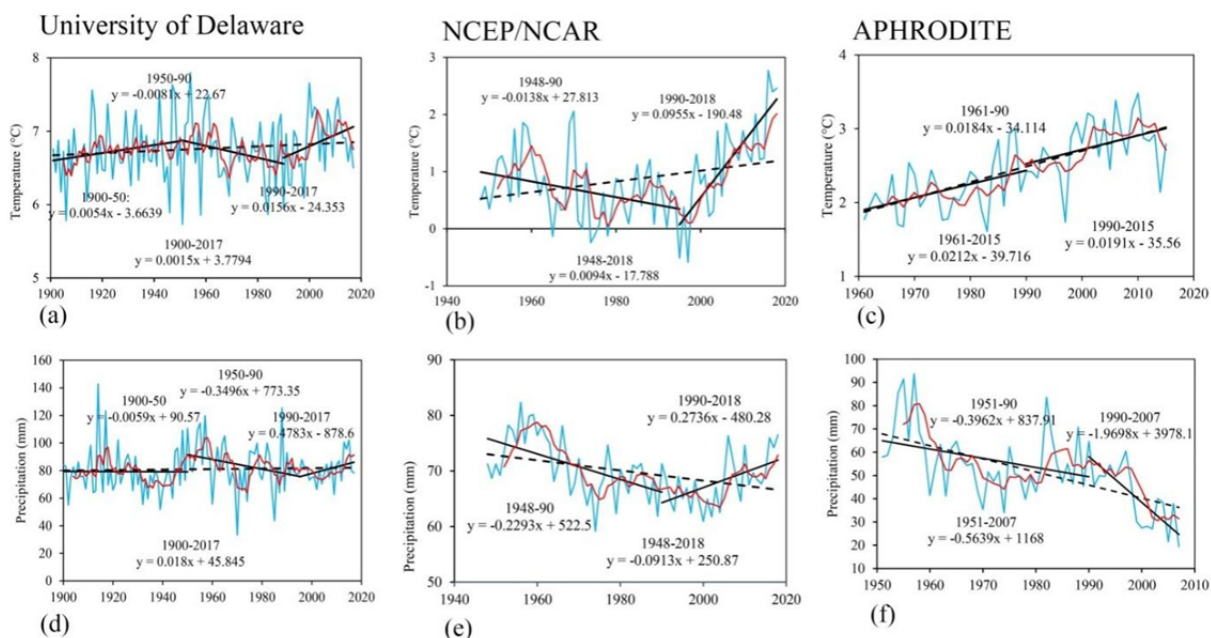

Fig. 11 Long-term trend of mean annual temperature (a-c) and precipitation (d-f) the part of western Himalaya analyzed from three different data sources. Red lines show the five-year moving average. The dotted line represents the overall trend for the entire observation. University of Delaware data provided by the NOAA/OAR/ESRL PSL, Boulder, Colorado, USA, from their website. NCEP Reanalysis Derived data provided by the NOAA/OAR/ESRL PSL, Boulder, Colorado, USA, from their website. APHRODITE datasets were downloaded from http://aphrodite.st.hirosaki-u.ac.jp/index.html.

Table 6 Comparison of glacier inventories for the Bhaga basin

Inventories	No.	Area (km²)	Min size (km²)	Year	Data source	*Spatial resol. (m)	References
ICIMOD	304	320.5	0.02	2005 ± 3	Landsat ETM+	30	Bajracharya and Shrestha 2011
RGI v6	304	366.7	0.02	2000 ± 2	Landsat ETM+	30	RGI Consortium 2017
GAMDAM	359	371.6	0.02	2001 ± 2	Landsat ETM+	30	Nuimura et al. 2015
Birajdar et al. 2014	231	385.9	0.03	2011	LISS III	24	Birajdar et al. 2014
Present study	306	360.3	0.02	2013	LISS IV, Google Earth imagery	5	

Note: * Spatial resol. = Spatial resolution
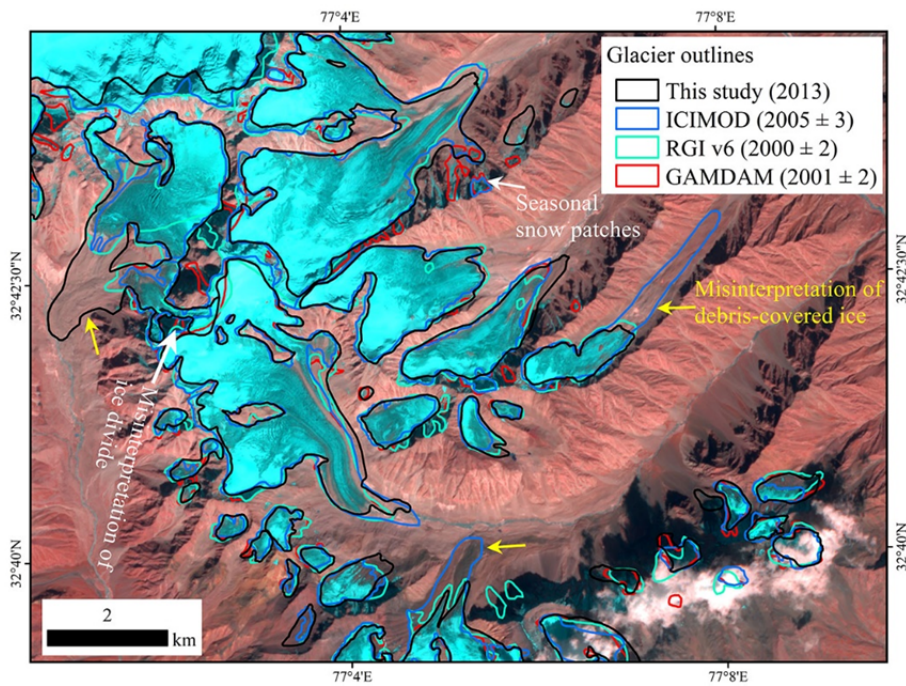
Fig. 12 Comparison of glacier inventories in the Bhaga basin. Sentinel 2 images (12−4−3 bands) were used as background. For details about the glacier inventories, see section 5.1.

inventories reveals large differences (Table 6): Birajdar et al. (2014) identified 231 glaciers (minimum mapping size of >0.03 km²) with a total area of 385.17 ± 3.71 km² in 2011. ICIMOD datasets (Bajracharya and Shrestha 2011) of 2005 ± 3 underestimate glacierized area by about 40 km² (11%), whereas according to the RGI inventory (RGI v6; 2000 ± 2) the glacier covered area amounts to 366.6 km² (RGI Consortium 2017) and is very similar to the presented study. The Glacier Area Mapping for Discharge from the Asian Mountains (GAMDAM) inventory overestimated the number by 53 with an area of 371.64 km² in 2001. These variations in glacier number and area might occur due to (i) misinterpretation of clean and debris-covered ice; (ii) temporal difference in image acquisitions and mapping; (iii) differences in mapping procedures (i.e.,

band ratios, manual delineation); (iv) misinterpretation of ice divide as a single entity (Fig. 12). A comparison with the inventory of the Geological Survey of India (GSI) based on topographic maps (SoI) and aerial photography is not possible, as digital glacier shapefiles are not available (Raina and Srivastava 2008).

Uncertainty in debris-covered glacier mapping depends on the spatial resolution of satellite images (Schmidt and Nüsser 2009; Bhambri et al. 2011; Chand and Sharma 2015; Schmidt and Nüsser 2017; Das and Sharma 2019; Nüsser and Schmidt 2021). For the case of Bhaga basin, the remote sensing approach was combined with field surveys in order to measure debris-covered terminus position with GPS and complemented by high-resolution 3D images from Google Earth. More than ten glaciers are being

monitored in the field on a regular basis over the last decades.

5.2 Comparison and differences in glacier changes with other study regions

The present study from the Bhaga basin indicates a much lower glacier recession rate (0.16 ± 0.03 % yr^{-1}) than previous change analysis using SoI maps (Table 1). For instance, Kulkarni et al. (2011) described a deglaciation rate of ~0.8 % yr^{-1} for Bhaga, ~0.5 % yr^{-1} for upper Chenab, ~0.2 % yr^{-1} for Miyar, and ~0.5 % yr^{-1} for Warwan between 1962 and 2001/2004 in the Chandrabhaga basin (Table 1). In the Warwan-Bhut region of the Chenab basin, Brahmbhatt et al. (2017) reported a glacier area loss of 11% (~0.3 % yr^{-1}) between 1962 and 2001. The higher rate of glacier decrease could result from an overestimation of

glacier cover in the SoI maps (Bhambri et al. 2011; Chand and Sharma 2015), which were used in both studies. Glaciers digitized from SoI maps and compared with outlines derived from Corona images (Fig. 13) show significant misinterpretation in the SoI maps (Fig. 13a). Thus, estimations based on SoI maps need to be cross-checked before being used in glacier change assessments and future modeling.

Other glacier change analysis exclusively based on remote sensing datasets supports the estimation described in this study: Birajdar et al. (2014) observed a retreat rate of 0.16 ± 0.1 % yr^{-1} from 2001 to 2011, and Pandey and Venkataraman (2013) reported a similar retreat rate of ~0.1 % yr^{-1} for 15 glaciers in the Chandrabhaga basin (1980−2010). During 1971−2016, Shukla and Garg (2019) reported a deglaciation (0.11 ± 0.04 % yr^{-1}) and recession rate (4.5 ± 2.5 m yr^{-1}) for the Panchi Nala glacier, confirmed in the present
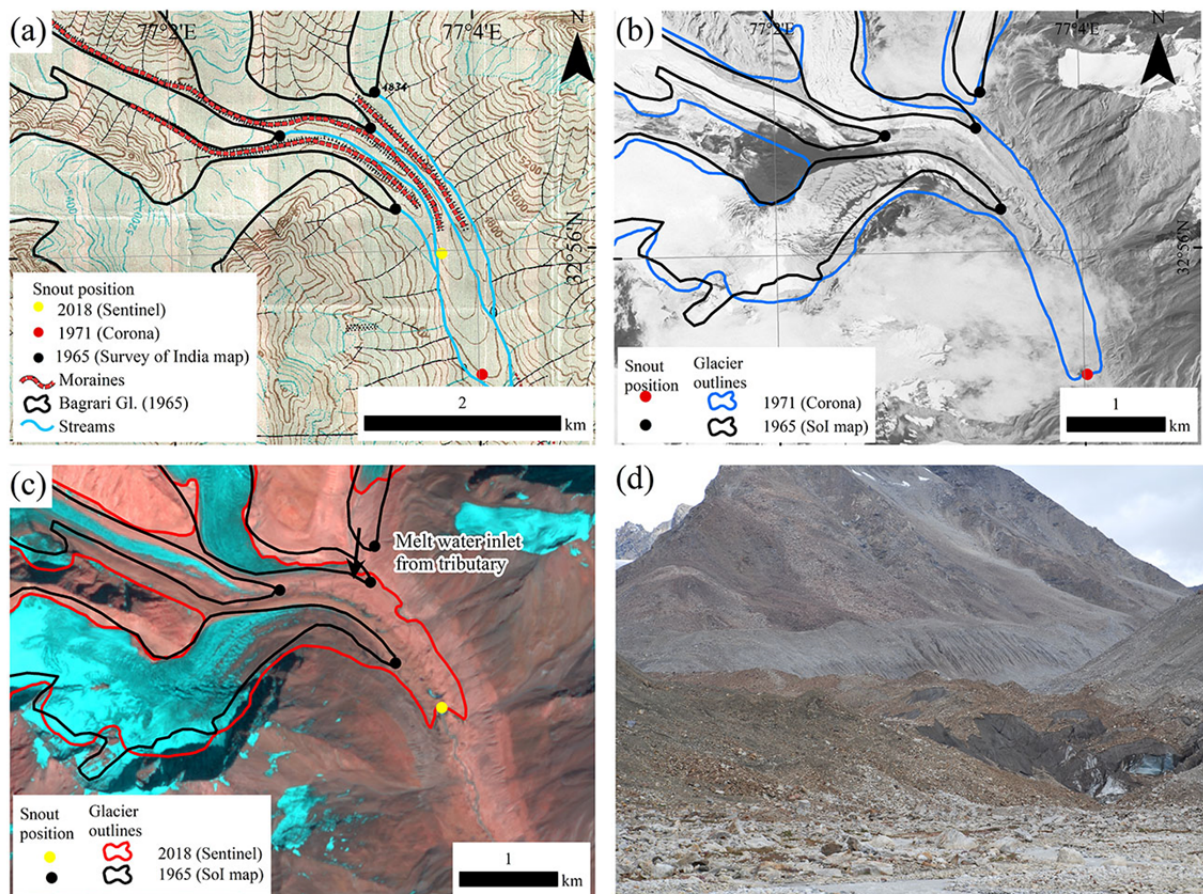
Fig. 13 Misinterpretation of glacier extents in the Survey of India (SoI) maps. An example is shown for the Bagrari Glacier in the Jankar Chhu watershed (JCW), Bhaga basin (see Fig. 1b for location). (a) The digitized Glacier outlines, snout positions, and meltwater streams on the SoI map of 1965. (b) Glacier outlines and snout positions for Corona (1971) and SoI map (1965) on Corona images. (c) SoI and Sentinel-derived glacier outlines overlaid on Sentinel 2 (12-4-3 bands) image. (d) Field photographs of the debris-covered ablation zone of Bagrari glacier in August 2018.

study (4.6 ± 0.5 m yr⁻¹). In the adjacent Miyar basin, a similar decreasing rate (~0.16 % yr⁻¹) was observed (Patel et al. 2018). In contrast, between 1971 and 2010 for the Baralacha glacier a larger deglaciation rate (~0.4 ± 0.1 % yr⁻¹) and a larger glacier retreat rate (10 m yr⁻¹) was observed by Negi et al. (2013). Furthermore, they identified a retreat of 9.3 m yr⁻¹ for Panchi Nala and 22.5 m yr⁻¹ for Zing-Zing Bar, both located in the BUW. Heterogeneity in glacier area change might be attributed to misinterpretation of debris-free and debris covered glaciers; temporal differences in terms of acquired images and mapping periods; differences in classification of glacier area; and adjacent ice masses may have been clubbed as single entities.

The comparison with other studies of the Himalaya indicates a higher decreasing rate in some regions. Thus, in the Western Himalaya (1962–2001), glaciers in the Baspa basin decreased at ~0.48 % yr⁻¹, in Parbati at ~0.56 % yr⁻¹, in Zanskar at ~0.23 % yr⁻¹, in Goriganga at ~0.48 % yr⁻¹ and in Bhagirathi at ~0.35 % yr⁻¹ (Kulkarni et al. 2011) (Appendix 18). In the Trans-Himalaya of Ladakh, a decreasing rate of ~0.35 % yr⁻¹ (1969–2010) was observed for the Kang Yatze (Schmidt and Nüsser 2012), with a higher rate for the longer observation period 1969–2016 of ~0.5 % yr⁻¹ for Kang Yatze, ~0.9 % yr⁻¹ for the Stok catchment, and ~0.4 % yr⁻¹ for the Lungsar range (Appendix 18) (Schmidt and Nüsser 2017). For the Central Ladakh range, Chudley et al. (2017) reported a slightly higher deglaciation rate of 0.55 % yr⁻¹ between 1991 and 2014. For the Eastern Himalaya of Bhutan, a much higher decreasing rate of about 0.8 % yr⁻¹ was observed between 1980 and 2010 (Bajracharya et al. 2014).

A number of other studies show similar decreasing trends as observed for the Bhaga basin. For the Nanga Parbat massif, located in the northwestern corner of the main Himalayan range, a glacier decrease of about 0.2 % yr⁻¹ was observed for the period 1990–2019, and 0.1 % yr⁻¹ from 1934–2019 (Nüsser and Schmidt 2021). Likewise, lower decreasing rates of about 0.1 ± 0.1 % yr⁻¹ were observed in the Ravi basin of the Himachal Himalaya for 1971–2013 (Chand and Sharma 2015). In the Saraswati/Alaknanda and Bhagirathi basins of the Garhwal Himalaya, the estimated glacier area loss amounted to 4.6 ± 2.8 % (~0.12 ± 0.1 % yr⁻¹) and 5.7 ± 2.7 % (~0.15 ± 0.1 % yr⁻¹) for 1968–2006, respectively (Bhambri et al. 2011). In the Khumbu Himalaya, glacier area loss amounted to 5.2 % (~0.12 % yr⁻¹) for

1962–2005 (Bolch et al. 2008; Appendix 18). The difference in deglaciation rate across the Himalayan region could be attributed to climatic differences, glacier nourishment and topographic setting, which are diverse for individual glaciers and for different basins (Hewitt 2011; Bhambri et al. 2012; Salerno et al. 2017).

5.3 Possible causes of heterogeneous glacier shrinkage

All studied glaciers in the Bhaga basin are shrinking during 1971–2020. However, the rate of change varies considerably between individual glaciers and watersheds. Studies from the western Himalayan region have reported strong warming trends in winter and weaker cooling in summer, and decreasing precipitation trends, suggesting a lower annual variability, one of the causes of glacial waning (Mukherjee et al. 2018; Das and Sharma 2019). Climate change is the primary driving force of glacier decrease, while local topographic factors may alter recession rates within a basin (Brun et al. 2019; Scherler et al. 2011a; Salerno et al. 2017; Zhang et al. 2022). The differences in deglaciation rate within the Bhaga basin could be attributed to the quantity and distribution of the clean and debris-covered ice, glacier size and length, hypsometric ice distribution, orientations of watersheds, geometry of the catchment topography, and nature and type of accumulation which may vary considerably for individual glaciers in the basin. The lower rate of area loss in the MV (-0.11 ± 0.03 % yr⁻¹) in comparison to the BUW (-0.27 ± 0.04 % yr⁻¹) during 1971–2020 can be explained by i) the larger mean glacier size in the MV (1.64 km²) compared to BUW (0.64 km²); ii) impact of a higher percentage of debris cover in the MV may have retard melting; iii) the glacier in the MV primarily orientated towards north-northwest directions while the majority of the clean glaciers in the BUW are south-southeast facing which may have accelerated melting due to the longer exposure of ice to sunlight.

In the Bhaga basin, glaciers <1 km² in size have lost 18.1 ± 2.6 % (0.3 ± 0.1 % yr⁻¹) of their area from 1971 to 2020. Previous Himalayan studies reported that relative changes of small glaciers were usually higher than in the case of large glaciers (Bhambri et al. 2011; Schmidt and Nüsser 2012; Chand and Sharma 2015; Das and Sharma 2019). In the Bhaga basin,

small glaciers with narrow elevation range lost a relatively higher percentage of their area, suggesting that smaller glaciers are inherently more sensitive to climate forcing than larger glaciers. Previous studies on western and central Himalayan glaciers also revealed a similar relationship between elevation range and frontal change (Bhambri et al. 2011; Das and Sharma 2019). Elevation and hypsometric ice distribution play a critical role in the response of the terminus to temperature changes (Jiskoot et al. 2009). Glaciers located at higher elevations are supposed to have lower deglaciation rates than those located at lower elevations due to temperature lapse rate. Considering the fact that large valley glaciers are characterized by longer response times (Jiskoot et al. 2009; Thakuri et al. 2014; Das and Sharma 2019; Nüsser and Schmidt 2021), glacier morphology, slope steepness, avalanche contribution, and large accumulation areas may accelerate ice movement to lower ablation zones and change retreat rates. Aspect broadly regulates the amount of direct solar energy distribution and direction of wind circulation (Jiskoot et al. 2009; Buri and Pellicciotti 2018). Generally, glaciers on northward-facing slopes receive less solar radiation and react more slowly as also observed in the Kang Yatze massif of Ladakh (Schmidt and Nüsser 2012). This highlights the importance of solar radiation and topographic shading on glaciers that may influence ice loss on the local scale.

A significant increase in debris-covered area was observed in all catchments of the Bhaga basin, probably attributed to a higher ratio of slopes that potentially supply debris in relation to the total glacier area (Das and Sharma 2019) or a relative increase of debris on the glacier surface in the process of downwasting (Schmidt and Nüsser 2009). Similar results of increasing debris coverage are also reported for the Bhagirathi basin in Garhwal (Bhambri et al. 2011). The presence of debris cover on Himalayan glaciers is a crucial surface property, as it modulates ablation rate (Scherler et al. 2011b; Rowan et al. 2015; Miles et al. 2018). Thick debris cover insulates the ice and reduces ablation (Hewitt 2005; Reznichenko et al. 2010), which allows glaciers to sustain at lower elevations than clean ice glaciers. The impact of debris cover on thermal properties of glaciers should be accounted for the analysis of spatially heterogeneous ice loss. In general, debris covered glaciers respond to warming by mass loss and thinning and not by drastic decrease in spatial extent

(Rowan et al. 2015). In the Bhaga basin lower deglaciation rate of debris covered glaciers (>30 % of area under debris cover; ~0.1 % yr^{-1}) were observed compared to debris-free ones (<10 % of area under debris; ~0.3 % yr^{-1}).

The presence of proglacial lakes enhances terminus disintegration by calving, and transmits thermal energy to ice, which accelerates the rate of area loss (Benn and Evans 2010; Basnett et al. 2013; Maurer at al. 2019). In the Koshi River basin of the central Himalaya, the area of debris covered glaciers with glacial lakes decreased faster than those without lakes, irrespective of size class (Xiang et al. 2018). A similar pattern can be observed in the Zanskar region (Shukla and Qadir 2016), in Sikkim (Basnett et al. 2013), and other parts of the central Himalaya (Sakai 2012). In the present study, the Bagrari glacier with the highest amount of debris cover (~2.5 km^2) and five supraglacial lakes retreated at the highest rate (25.3 m yr^{-1}). In front of the Mayar II glacier, one proglacial lake has emerged between 2000 and 2020 (Appendix 19), resulting in faster glacier retreat in recent decades.

Three different types of climate datasets were used to evaluate the climatic trend for the Bhaga basin during the last century. In the present study, APHRODITE provides better temperature and precipitation estimates compared to other studies from the western Himalaya. According to Bao & Zhang (2013), APHRODITE data provides better precipitation estimates than NCEP/NCAR data in relatively flat terrain. Comparison between different climatic datasets is not feasible due to their different spatial resolution (i.e., 2.5° (~277 km^2) for NCEP/NCAR and 0.5° (~55 km^2) for APHRODITE) and models used for interpolation. NCEP/NCAR dataset covers a vast area spanning from the monsoon-dominated Pir-Panjal range in south to the arid Trans-Himalayan range in north (Appendix 20), while APHRODITE data gives more precise estimates due to low ground coverage. This possibly leads to a contrary trend of precipitation among datasets. Here, we consider APHRODITE as the most suitable climatic model to interpret glacier change in the mountainous region as reported by other studies (Mukherjee et al. 2018; Kaushik et al. 2020). In the Western Himalaya the annual maximum temperature (T_{MAX}) increased by 2.8 °C and the minimum temperature (T_{MIN}) by 1 °C (Shekhar et al. 2010). In contrast, Dash et al. (2007) mentioned a decrease of

T_{MIN} by 1.9 °C during 1955–1972. The analysis of NCEP/NCAR data shows that MAT increased by ~0.6 °C between 1948 and 2018, while APHRODITE data reveals an increase of 1.1 °C during 1961–2015. The presented results of climatic data show warming trends in winter and cooling in summer months between 1961 and 2015. In addition, a significant decreasing trend in precipitation was observed from APHRODITE data since the 1990s. Mukherjee et al. (2018) reported a similar shift in climatic parameters based on multiple gridded datasets from the adjacent upper Chandra basin. Based on these climatic trends, it can be assumed that the loss of glacier surface area in the Bhaga basin between 1971 and 2020 reflects the combined influence of rising trends in temperature and declining trends in precipitation. In the present study, a higher area loss rate (~0.23 ± 0.02 % yr^{-1}) was observed in the last two decades (2000–2020) as compared to earlier decades (~0.15 ± 0.01 % yr^{-1}; 1971–2000). The combination of rising temperature and declining precipitation controls recent glacier decrease in the Bhaga basin.

6 Conclusion

This study provides a comprehensive updated glacier inventory and multitemporal glacier change records for the Bhaga basin in the western Himalaya over the last five decades (1971–2020). Based on remote sensing and field surveys, this study suggests that earlier assessments exclusively based on SoI topographic maps were erroneously overestimating regional glacier decrease. Therefore, a reassessment for all those areas where SoI maps have been used for glacier inventories of the 1960s is strongly recommended. For this purpose, Corona images offer a valuable possibility to map glacier outlines of the ~1960s. The glaciological community will benefit by storing and using remote sensed glacier outlines in a GIS platform to perform spatial and temporal analyses at different scales, valuable for basin-scale glaciological and hydrological modeling. In addition, the availability of long-term instrumental climatic records and field-based measurements (e.g., mass balance, debris cover thickness) within the basin will provide a valuable database and further improve knowledge of glacier change and corresponding interactions to ongoing climate change.

Electronic supplementary material: Supplementary material (Appendixes 1-20) is available in the online version of this article at https://doi.org/10.1007/s11629-022-7598-9

References

Armstrong RL, Rittger K, Brodzik MJ, et al (2019) Runoff from glacier ice and seasonal snow in High Asia: separating melt water sources in river flow. Reg Environ Change 19:1249–1261.
https://doi.org/10.1007/s10113-018-1429-0

Bajracharya B, Shrestha SR (2011) The Status of Glaciers in the Hindu Kush–Himalayan Region. ICIMOD.

Bajracharya SR, Maharjan SB, Shrestha F (2014) The status and decadal change of glaciers in Bhutan from the 1980s to 2010 based on satellite data. Ann Glaciol 55:159–166.
https://doi.org/10.3189/2014AoG66A125

Bao X, Zhang F (2013) Evaluation of NCEP-CFSR, NCEP-NCAR, ERA-Interim, and ERA-40 reanalysis datasets against independent sounding observations over the Tibetan Plateau. J Clim 26:206–214.
https://doi.org/10.1175/JCLI-D-12-00056.1

Basnett S, Kulkarni AV, Bolch T (2013) The influence of debris cover and glacial lakes on the recession of glaciers in Sikkim Himalaya, India. J Glaciol 59:1035–1046.
https://doi.org/10.3189/2013JoG12J184

Benn DI, Evans DJA (2010) Glaciers and Glaciation. Hodder Education, London.

Bhambri R, Bolch T, Chaujar RK (2012) Frontal recession of Gangotri Glacier, Garhwal Himalayas, from 1965 to 2006, measured through highresolution remote sensing data. Curr Sci 102:489–494.
https://doi.org/10.5167/uzh-59630

Bhambri R, Bolch T, Chaujar RK, Kulshreshtha SC (2011) Glacier changes in the Garhwal Himalaya, India, from 1968 to 2006 based on remote sensing. J Glaciol 57:543–556.
https://doi.org/10.3189/002214311796905604

Birajdar F, Venkataraman G, Bahuguna I, Samant H (2014) A Revised Glacier Inventory of Bhaga Basin Himachal Pradesh, India: Current Status and Recent Glacier Variations. ISPRS Ann Photogramm Remote Sens Spat Inf Sci II–8:37–43.
https://doi.org/10.5194/isprsannals-II-8-37-2014

Bolch T, Buchroithner M, Pieczonka T, Kunert A (2008) Planimetric and volumetric glacier changes in the Khumbu Himal, Nepal, since 1962 using Corona, Landsat TM and ASTER data. J Glaciol 54:592–600.
https://doi.org/10.3189/002214308786570782

Bolch T, Kulkarni A, Kääb A, et al (2012) The state and fate of himalayan glaciers. Sci 336:310–314.
https://doi.org/10.1126/science.1215828

Bolch T, Menounos B, Wheate R (2010) Landsat-based inventory of glaciers in western Canada , 1985 – 2005. Remote Sens Environ 114:127–137.
https://doi.org/10.1016/j.rse.2009.08.015

Bolch T, Shea JM, Liu S, et al (2019) Status and change of the cryosphere in the extended Hindu Kush Himalaya Region. In: Wester P, Mishra A, Mukherji A, Shrestha AB (eds) The Hindu Kush Himalaya assessment: mountains, climate change, sustainability and people. Springer International Publishing, Cham, pp 209–255.

Brahmbhatt RM, Bahuguna IM, Rathore BP, et al (2017) Significance of glacio-morphological factors in glacier retreat: a case study of part of Chenab basin, Himalaya. J Mt Sci 14:128–141.
https://doi.org/10.1007/s11629-015-3548-0

Brun F, Wagnon P, Berthier E, et al (2019) Heterogeneous Influence of Glacier Morphology on the Mass Balance Variability in High Mountain Asia. J Geophys Res Earth Surf 124:1331–1345.
https://doi.org/10.1029/2018JF004838

Buri P, Pellicciotti F (2018) Aspect controls the survival of ice cliffs on debris-covered glaciers. Proc Natl Acad Sci 115:1–23.
https://doi.org/10.1073/pnas.1713892115

Chand P, Sharma MC (2015) Glacier changes in the Ravi basin, North-Western Himalaya (India) during the last four decades (1971-2010/13). Glob Planet Change 135:133–147.
https://doi.org/10.1016/j.gloplacha.2015.10.013

Chand P, Sharma MC, Bhambri R, et al (2017) Reconstructing the pattern of the Bara Shigri Glacier fluctuation since the end of the Little Ice Age, Chandra valley, north-western Himalaya. Prog Phys Geogr 41:643–675.
https://doi.org/10.1177/0309133317728017

Chudley TR, Miles ES, Willis IC (2017) Glacier characteristics and retreat between 1991 and 2014 in the Ladakh range, Jammu and Kashmir. Remote Sens Lett 8:518–527.
https://doi.org/10.1080/2150704X.2017.1295480

Das S, Sharma MC (2019) Glacier changes between 1971 and 2016 in the Jankar Chhu Watershed, Lahaul Himalaya, India. J Glaciol 65:13–28.
https://doi.org/10.1017/jog.2018.77

Das S, Sharma MC, Murari MK (2022) Spatially heterogeneous glacier elevation change in the Jankar Chhu Watershed, Lahaul Himalaya, India derived using ASTER DEMs. Geocarto Int 0:1–27.
https://doi.org/10.1080/10106049.2022.2136254

Dash SK, Jenamani RK, Kalsi SR, Panda SK (2007) Some evidence of climate change in twentieth-century India. Clim Change 85:299–321.
https://doi.org/10.1007/s10584-007-9305-9

Farinotti D, Immerzeel WW, de Kok RJ, et al (2020) Manifestations and mechanisms of the Karakoram glacier Anomaly. Nat Geoscience 13:8–16.
https://doi.org/10.1038/s41561-019-0513-5

Frey H, Paul F, Strozzi T (2012) Compilation of a glacier inventory for the western Himalayas from satellite data: Methods, challenges, and results. Remote Sens Environ 124:832–843.
https://doi.org/10.1016/j.rse.2012.06.020

Gardelle J, Arnaud Y, Berthier E (2011) Contrasted evolution of glacial lakes along the Hindu Kush Himalaya mountain range between 1990 and 2009. Glob Planet Change 75:47–55.
https://doi.org/10.1016/j.gloplacha.2010.10.003

Hall DK, Bayr KJ, Schöner W, et al (2003) Consideration of the errors inherent in mapping historical glacier positions in Austria from the ground and space (1893-2001). Remote Sens Environ 86:566–577.
https://doi.org/10.1016/S0034-4257(03)00134-2

Herreid S, Pellicciotti F (2020) The state of rock debris covering Earth's glaciers. Nat Geoscience 13:621–627.
https://doi.org/10.1038/s41561-020-0615-0

Hewitt K (2005) The Karakoram Anomaly? Glacier Expansion and the 'Elevation Effect,' Karakoram Himalaya. Mt Res Dev 25:332–340.
https://doi.org/10.1659/0276-4741(2005)025[0332:TKAGEA]2.0.CO;2

Hewitt K (2011) Glacier Change, Concentration, and Elevation Effects in the Karakoram Himalaya, Upper Indus Basin. Mt Res Dev 31:188–200.
https://doi.org/10.1659/MRD-JOURNAL-D-11-00020.1

Hock R, Rasul G, C. Adler, et al (2019) High Mountain Areas. In Pörtner HO, Roberts DC, Masson-Delmotte V, Zhai P, Tignor M, Poloczanska E, Mintenbeck K, Nicolai M, Okem A, Petzold J, Rama B, Weyer N, editors, The Ocean and Cryosphere in a Changing Climate. Intergovernmental Panel on Climate

Change. p. 2-1 - 290.

Immerzeel WW, Beek LPH van, Bierkens MFP (2010) Climate Change Will Affect the Asian Water Towers. Sci 328:1382–1385.
https://www.science.org/doi/10.1126/science.1183188

Jiskoot H, Curran CJ, Tessler DL, Shenton LR (2009) Changes in Clemenceau Icefield and Chaba Group glaciers, Canada, related to hypsometry, tributary detachment, length-slope and area-aspect relations. Ann Glaciol 50:133–143.
https://doi.org/10.3189/172756410790595796

Kääb A, Treichler D, Nuth C, Berthier E (2015) Brief Communication: Contending estimates of 2003–2008 glacier mass balance over the Pamir–Karakoram–Himalaya. Cryosphere 9:557–564.
https://doi.org/10.5194/tc-9-557-2015

Kalnay E, Kanamitsu M, Kistler R, et al (1996) The NCEP/NCAR 40-year reanalysis project. Bull Amer Meteor 77:437–471.
https://doi.org/10.1175/1520-0477(1996)077<0437:TNYRP>2.0.CO;2

Kaushik S, Dharpure JK, Joshi PK, et al (2020) Climate change drives glacier retreat in Bhaga basin located in Himachal Pradesh, India. Geocarto Int 35:1179–1198.
https://doi.org/10.1080/10106049.2018.1557260

Koblet T, Gärtner-Roer I, Zemp M, et al (2010) Reanalysis of multi-temporal aerial images of Storglaciren, Sweden (1959-99) - Part 1: Determination of length, area, and volume changes. Cryosphere 4:333–343.
https://doi.org/10.5194/tc-4-333-2010

Kulkarni A V., Bahuguna IM, Rathore BP, et al (2007) Glacial retreat in Himalayas using Indian remote sensing satellite data. Curr Sci 92:69–74.
https://doi.org/10.1117/12.694004

Kulkarni A V, Rathore BP, Singh SK, Bahuguna IM (2011) Understanding changes in the Himalayan cryosphere using remote sensing techniques. Int J Remote Sens 32:601–615.
https://doi.org/10.1080/01431161.2010.517802

Legates DR, Willmott CJ (1990) Mean seasonal and spatial variability in global surface air temperature. Theor Appl Climatol 41:11–21.
https://doi.org/10.1007/BF00866198

Lopez P, Chevallier P, Favier V, et al (2010) A regional view of fluctuations in glacier length in southern South America. Glob Planet Change 71:85–108.
https://doi.org/10.1016/j.gloplacha.2009.12.009

Machguth H, Huss M (2014) The length of the world's glaciers - a new approach for the global calculation of center lines. Cryosphere 8:1741–1755.
https://doi.org/10.5194/tc-8-1741-2014

Maurer JM, Schaefer JM, Rupper S, Corley A (2019) Acceleration of ice loss across the Himalayas over the past 40 years. Sci Adv 5: eaav7266.
https://doi.org/10.1126/sciadv.aav7266

Mayewski PA, Jeschke PA (1979) Himalayan and Trans-Himalayan Glacier Fluctuations since AD 1812. Arct Antarct Alp Res 11:267–287.
https://doi.org/10.2307/1550417

Mergili M, Müller JP, Schneider JF (2013) Spatio-temporal development of high-mountain lakes in the headwaters of the Amu Darya River (Central Asia). Glob Planet Change 107:13–24.
https://doi.org/10.1016/j.gloplacha.2013.04.001

Miles KE, Hubbard B, Quincey DJ, et al (2018) Polythermal structure of a Himalayan debris-covered glacier revealed by borehole thermometry. Sci Rep 8:1–9.
https://doi.org/10.1038/s41598-018-34327-5

Mir RA, Jain SK, Jain SK, et al (2017) Assessment of Recent Glacier Changes and Its Controlling Factors from 1976 to 2011 in Baspa Basin, Western Himalaya. Arct Antarct, Alp Res 49:621–647.
https://doi.org/10.1657/AAAR0015-070

Muhammad S, Tian L, Nüsser M (2019) No significant mass loss in the glaciers of Astore Basin (North-Western Himalaya), between 1999 and 2016. J Glaciol 65:270–278.
https://doi.org/10.1017/jog.2019.5

Mukherjee K, Bhattacharya A, Pieczonka T, et al (2018) Glacier mass budget and climate reanalysis data indicate a climatic shift around 2000 in Lahaul-Spiti, western Himalaya. Clim Change 148:219–233.
https://doi.org/10.1007/s10584-018-2185-3

Murtaza KO, Romshoo SA (2017) Recent glacier changes in the Kashmir Alpine Himalayas, India. Geocarto Int 32:188–205.
https://doi.org/10.1080/10106049.2015.1132482

Negi HS, Saravana G, Rout R, Snehmani (2013) Monitoring of great Himalayan glaciers in Patsio region, India using remote sensing and climatic observations. Curr Sci 105:1383–1392.

Nuimura T, Sakai A, Taniguchi K, et al (2015) The GAMDAM glacier inventory: A quality-controlled inventory of Asian glaciers. Cryosphere 9:849–864.
https://doi.org/10.5194/tc-9-849-2015

Nüsser M, Baghel R (2014) The Emergence of the Cryoscape: Contested Narratives of Himalayan Glacier Dynamics and Climate Change. In: Schuler B (ed) Environmental and Climate Change in South and Southeast Asia. Brill, Leiden, pp 138–156.

Nüsser M, Schmidt S (2021) Glacier changes on the Nanga Parbat 1856–2020: A multi-source retrospective analysis. Sci Total Environ 785:147321.
https://doi.org/10.1016/j.scitotenv.2021.147321

Pandey P, Venkataraman G (2013) Change in glaciers in Chandra-Bhaga basin, Himachal Himalaya, India, between 1980 and 2010 measured using remote sensing. Int J Remote Sens 34:5584–5597.
https://doi.org/10.1080/01431161.2013.793464

Patel LK, Sharma P, Fathima TN, Thamban M (2018) Geospatial observations of topographical control over the glacier retreat, Miyar basin, Western Himalaya, India. Environ Earth Sci 77:1–12.
https://doi.org/10.1007/s12665-018-7379-5

Paul F, Barrand NE, Baumann S, et al (2013) On the accuracy of glacier outlines derived from remote-sensing data. Ann Glaciol 54:171–182.
https://doi.org/10.3189/2013AoG63A296

Racoviteanu AE, Arnaud Y, Williams MW, Manley WF (2015) Spatial patterns in glacier characteristics and area changes from 1962 to 2006 in the Kanchenjunga-Sikkim area, eastern Himalaya. Cryosphere 9:505–523.
https://doi.org/10.5194/tc-9-505-2015

Raina VK, Srivastava D (2008) Glaciers atlas of India, First ed. Geological society of India, Bangalore.

Reznichenko N, Davies T, Shulmeister J, McSaveney M (2010) Effects of debris on ice-surface melting rates: An experimental study. J Glaciol 56:384–394.
https://doi.org/10.3189/002214310792447725

RGI Consortium (2017) Randolph Glacier Inventory – A Dataset of Global Glacier Outlines: Version 6.0: Technical Report, Global Land Ice Measurements from Space. Boulder, Colorado USA. NSIDC: National Snow and Ice Data Center.
https://doi.org/10.7265/4m1f-gd79

Rowan AV (2017) The 'Little Ice Age' in the Himalaya: A review of glacier advance driven by Northern Hemisphere temperature change. Holocene 27:292–308.
https://doi.org/10.1177/0959683616658530

Rowan A V., Egholm DL, Quincey DJ, Glasser NF (2015)

Modelling the feedbacks between mass balance, ice flow and debris transport to predict the response to climate change of debris-covered glaciers in the Himalaya. Earth Planet Sci Lett 430:427–438.
https://doi.org/10.1016/j.epsl.2015.09.004

Sakai A (2012) Glacial Lakes in the Himalayas: A Review on Formation and Expansion Processes. Glob Environ Res 16:23–30.

Salerno F, Thakuri S, Tartari G, et al (2017) Debris-covered glacier anomaly? Morphological factors controlling changes in the mass balance, surface area, terminus position, and snow line altitude of Himalayan glaciers. Earth Planet Sci Lett 471:19–31.
https://doi.org/10.1016/j.epsl.2017.04.039

Scherler D, Bookhagen B, Strecker MR (2011a) Hillslope- glacier coupling: The interplay of topography and glacial dynamics in High Asia. J Geophys Res 116:1–21.
https://doi.org/10.1029/2010JF001751

Scherler D, Bookhagen B, Strecker MR (2011b) Spatially variable response of Himalayan glaciers to climate change affected by debris cover. Nat Geoscience 4:156–159.
https://doi.org/10.1038/ngeo1068

Scherler D, Wulf H, Gorelick N (2018) Global Assessment of Supraglacial Debris-Cover Extents. Geophys Res Lett 45:11,798-11,805.
https://doi.org/10.1029/2018GL080158

Schmidt S, Nüsser M (2017) Changes of High-Altitude Glaciers in the Trans-Himalaya of Ladakh over the Past Five Decades (1969 – 2016). Geosciences 7:469–506.
https://doi.org/10.3390/geosciences7020027

Schmidt S, Nüsser M (2012) Changes of High Altitude Glaciers from 1969 to 2010 in the Trans-Himalayan Kang Yatze Massif, Ladakh, Northwest India. Antarct Alp Res 44:107–121.
https://doi.org/10.1657/1938-4246-44.1.107

Schmidt S, Nüsser M (2009) Fluctuations of Raikot glacier during the past 70 years: A case study from the Nanga Parbat massif, northern Pakistan. J Glaciol 55:949–959.
https://doi.org/10.3189/002214309790794878

Schmidt S, Nüsser M, Baghel R, Dame J (2020) Cryosphere hazards in Ladakh: the 2014 Gya glacial lake outburst flood and its implications for risk assessment. Nat Hazards 104:2071–2095.
https://doi.org/10.1007/s11069-020-04262-8

Shekhar MS, Chand H, Kumar S, et al (2010) Climate-change studies in the western Himalaya. Ann Glaciol 51:105–112.
https://doi.org/10.3189/172756410791386508

Shukla A, Garg PK (2019) Evolution of a debris-covered glacier in the western Himalaya during the last four decades (1971–2016): A multiparametric assessment using remote sensing and field observations. Geomorphology 341:1–14.
https://doi.org/10.1016/j.geomorph.2019.05.009

Shukla A, Garg PK, Srivastava S (2018) Evolution of glacial and high-altitude lakes in the Sikkim, Eastern Himalaya over the past four decades (1975-2017). Front Environ Sci 6:1–19.
https://doi.org/10.3389/fenvs.2018.00081

Shukla A, Qadir J (2016) Differential response of glaciers with varying debris cover extent: evidence from changing glacier parameters. Int J Remote Sens 37:2453–2479.
https://doi.org/10.1080/01431161.2016.1176272

Thakuri S, Salerno F, Smiraglia C, et al (2014) Tracing glacier changes since the 1960s on the south slope of Mt. Everest (central Southern Himalaya) using optical satellite imagery. Cryosphere 8:1297–1315.
https://doi.org/10.5194/tc-8-1297-2014

Xiang Y, Yao T, Gao Y, et al (2018) Retreat rates of debris-covered and debris free glaciers in the Koshi River Basin, central Himalayas, from 1975 to 2010. Environ Earth Sci 77:1–13.
https://doi.org/10.1007/s12665-018-7457-8

Yatagai A, Kamiguchi K, Arakawa O, et al (2012) Aphrodite constructing a long-term daily gridded precipitation dataset for Asia based on a dense network of rain gauges. Bull Amer Meteor 93:1401–1415.
https://doi.org/10.1175/BAMS-D-11-00122.1

Zhang G, Yao T, Xie H, et al (2015) An inventory of glacial lakes in the Third Pole region and their changes in response to global warming. Glob Planet Change 131:148–157.
https://doi.org/10.1016/j.gloplacha.2015.05.013

Zhang Z, Gu Z, Hu K, et al (2022) Spatial variability between glacier mass balance and environmental factors in the High Mountain Asia. J Arid Land 14:441–454.
https://doi.org/10.1007/s40333-017-0014-z